

Genetic, Genomic, and Functional Analysis of the Granule Lattice Proteins in *Tetrahymena* Secretory Granules

Andrew T. Cowan,^{*†} Grant R. Bowman,^{*†} Kyle F. Edwards,^{*} J. J. Emerson,[‡] and Aaron P. Turkewitz^{*}

Departments of ^{*}Molecular Genetics and Cell Biology and [‡]Ecology and Evolution, The University of Chicago, Chicago, IL 60637

Submitted January 18, 2005; Revised April 27, 2005; Accepted June 3, 2005
Monitoring Editor: Randy Schekman

In some cells, the polypeptides stored in dense core secretory granules condense as ordered arrays. In ciliates such as *Tetrahymena thermophila*, the resulting crystals function as projectiles, expanding upon exocytosis. Isolation of granule contents previously defined five Granule lattice (Grl) proteins as abundant core constituents, whereas a functional screen identified a sixth family member. We have now expanded this screen to identify the nonredundant components required for projectile assembly. The results, further supported by gene disruption experiments, indicate that six *Grl* proteins define the core structure. Both in vivo and in vitro data indicate that core assembly begins in the endoplasmic reticulum with formation of specific hetero-oligomeric Grl proprotein complexes. Four additional *GRL*-like genes were found in the *T. thermophila* genome. *Grl2p* and *Grl6p* are targeted to granules, but the transcripts are present at low levels and neither is essential for core assembly. The Δ *GRL6* cells nonetheless showed a subtle change in granule morphology and a marked reduction in granule accumulation. Epistasis analysis suggests this results from accelerated loss of Δ *GRL6* granules, rather than from decreased synthesis. Our results not only provide insight into the organization of Grl-based granule cores but also imply that the functions of Grl proteins extend beyond core assembly.

INTRODUCTION

Dense core granules (DCGs) are vesicles specialized for storage of highly concentrated proteins, which can be secreted via exocytic fusion with the plasma membrane in response to extracellular stimuli (Arvan and Castle, 1992; Arvan and Castle, 1998). The cargo itself, rather than functioning as a mere passenger in this pathway, seems to play a central role in driving granule formation (Arvan *et al.*, 2002). The mechanisms involved may involve biophysical properties of DCG proteins, including reversible aggregation in response to changes in the ionic composition between successive compartments of the secretory pathway (Chanat and Huttner, 1991). In addition to such conditional solubility, some DCG cargo proteins may interact with the lipid bilayer in noncanonical ways that also may be important for sorting (Dhanvantari and Loh, 2000; Tooze *et al.*, 2001). For these reasons, simply identifying the DCG cargo is an important first step in analyzing granule biogenesis in any specific cell type.

An additional motivation for defining granule cargo exists in the ciliates, single-celled protists that as a group synthesize a variety of DCGs (Rosati and Modeo, 2003). DCG formation in ciliates involves the organization of luminal cargo proteins as large crystals, which have the remarkable property of undergoing spring-like expansion upon exocytosis in a way that ensures rapid content release (Hausmann, 1978). The assembly of such reproducible crystalline structures within the secretory pathway poses interesting regulatory questions, for example, with regard to nucleation and size control. Molecular analysis of DCGs in ciliates has been chiefly limited to two organisms, *Tetrahymena thermophila* and *Paramecium tetraurelia* (Vayssie *et al.*, 2000; Turkewitz, 2004). In the latter, biochemical isolation of granules and protein microsequencing led to cloning of the trichocyst matrix proteins (tmpts). These fell into three families that together may include >100 members and that may all adopt a similar overall structure (Madeddu *et al.*, 1995; Gautier *et al.*, 1996). Localization and gene silencing studies provided evidence that *Paramecium* granule cores were multilayered constructs in which distinct tmp families independently assembled into concentric zones (Vayssie *et al.*, 2001). For example, cells in which the T1 tmp family members were silenced still formed an ordered, central core plug, but they lacked the overlying structure found in wild-type granules.

DCGs in *Tetrahymena* seem morphologically and chemically less complex than those in *Paramecium*. The tmp homologues in *T. thermophila* were named granule lattice (Grl) proteins, and five members were initially identified starting with isolation of the most abundant DCG contents (Chilcoat *et al.*, 1996). Biochemical analysis of *Grl1p* indicated that conformational changes could underlie the crystalline expansion noted above, whereas gene disruption suggested that *Grl1p* itself might be present throughout the entire core, because no visibly ordered structure was formed in its absence (Verbsky and Turkewitz, 1998). Granules formed in such Δ *GRL1* cells did not undergo rapid expansion upon exocytosis (Chilcoat *et al.*, 1996). This defect, due to the absence of a single granule protein, facilitated an entirely different approach to identifying granule contents based on

This article was published online ahead of print in *MBC in Press* (<http://www.molbiolcell.org/cgi/doi/10.1091/mbc.E05-01-0028>) on June 15, 2005.

[†] These authors contributed equally to this work.

Address correspondence to: Aaron P. Turkewitz (apturkew@midway.uchicago.edu).

screening for exocytosis-defective mutants among cells transformed with an antisense library, a technique allowing phenotype-based gene cloning in this organism (Sweeney *et al.*, 1996). This identified a sixth family member, initially called *NDC1* (for nondischarge) but here renamed *GRL8* for simplicity (Chilcoat *et al.*, 2001). Granules lacking *Grl8p*, like those lacking *Grl1p*, had no discernibly organized structure. The *tmp/Grl* family of proteins have no identified homologues outside of ciliates, but they are nonetheless similar to abundant dense core granule proteins in animal cells, called chromogranins, in having a preponderance of acidic amino acids, which endow them with the capacity to bind calcium (Chanat *et al.*, 1991).

In the work presented here, we have extended the initial genetic screening to ask whether other genes were required for core formation. The results provided strong evidence that the family of six *Grl* proteins represents the essential structural core components in this organism. At the same time, searching the *T. thermophila* macronuclear genome revealed four additional paralogs, named *GRL2*, *6*, *9*, and *10*. We have undertaken functional analysis of a large subset of the *GRL* family. The results confirm that six *GRL* genes (*GRL1*, *3*, *4*, *5*, *7*, and *8*) each play a nonredundant role in core formation. The assembly defects associated with individual disruption of *GRL1*, *3*, *4*, *7*, and *8* are similar, suggesting that each may contribute to a common structural unit. In support of this, we present evidence that some *Grl* proteins assemble into hetero-oligomeric complexes in the endoplasmic reticulum (ER) and that assembly may be required for ER exit. The products of *GRL2* and *6* are much less abundant and not essential for lattice formation. Nonetheless, disruption of *GRL6* had effects on both granule morphology and number, indicating a novel role for this gene product.

MATERIALS AND METHODS

Cell Strains and Culture

Strain CU428.1, *MPR^R/MPR^R* (6-methylpurine-sensitive, VII) bears a dominant allele conferring 6-methylpurine resistance in the micronucleus and the corresponding sensitive allele in the macronucleus; strain B2086, *mpr^S/mpr^S* (6-methylpurine-sensitive, II) has the drug-sensitive allele in both nuclei. Both were provided by Peter Bruns (Cornell University, Ithaca, NY). Cells were grown at 30°C with agitation in 2% proteose peptone, 0.2% yeast extract (both from Difco, Detroit, MI), with 0.009% ferric EDTA. For viewing of green fluorescent protein (GFP)-tagged proteins, cells were grown in 0.2% yeast extract with 0.009% ferric EDTA, to reduce autofluorescence. Unless stated otherwise, reagents were obtained from Sigma-Aldrich (St. Louis, MO).

Gene Disruption

Genes were disrupted by first using a selectable marker to replace a large region of a cloned copy. The marker consisted of the NEO gene on an autonomous expression cassette (Gaertig *et al.*, 1994). The cloned interrupted copy was then introduced into *Tetrahymena*, to integrate via homologous recombination. *GRL3* was disrupted by replacement by the NEO2 cassette of the sequences -154 to 1526 (these junctions determined by convenient restriction sites) relative to the start codon. Similarly, *GRL4* was disrupted by replacement of the sequences -310 to 727 with NEO2. *GRL7* was disrupted by replacement of the sequences 1-2402 with a similar cassette, MTT-NEO. The difference between NEO2 and MTT-NEO is that the former uses a histone H4 promoter, whereas the latter uses an inducible metallothionein (*MTT1*) promoter, to drive expression of the gene responsible for drug resistance (Shang *et al.*, 2002). Disruptions were accomplished by biolistic transformation of CU428.1, as described previously (Chilcoat *et al.*, 1996). Initial drug selection was with 120 µg/ml paromomycin, added 6 h after transformation. Cells transformed with the *GRL7* disruption construct were grown in 0.5 µg/ml CdCl₂ immediately after transformation and during the entire period of drug selection to induce the *MTT1* promoter. Because only some of the macronuclear copies of the target gene are replaced initially, cells were cultured with increasing concentrations of paromomycin (up to 800 µg/ml) and allowed to grow for >60 generations for stringent selection of the disrupted allele.

Western Blotting

To make whole cell lysates, ~8 × 10⁵ cells were pelleted for 30 s in a clinical centrifuge and reduced to a volume of 250 µl before adding an equal volume of 100°C 2 × SDS-PAGE sample buffer (final concentration 100 mM sucrose, 3% SDS, 2 mM Na₂EDTA, and 62.5 mM Tris, pH 6.9) and boiled for 3 min. For Western blots, 12 µl of lysate was electrophoresed using SDS-PAGE and transferred to 0.45-µm nitrocellulose (Osmonics, Westborough, MA). Immunoblots with polyclonal antisera were blocked, probed, and washed with 5% milk in tris-buffered saline (TBS). The anti-*Grl1p*, anti-*Grl3p*, anti-*Grl4p*, and anti-*Grl8p* antibodies were used at 1:1000, 1:400, 1:250, and 1:1500, respectively. Detection of primary antibodies was with horseradish peroxidase-conjugated goat anti-rabbit antibody at 1:2000 (Jackson ImmunoResearch Laboratories, West Grove, PA); blots were developed with Pierce Supersignal (Pierce Chemical, Rockford, IL) and exposed to film.

Immunofluorescence and Microscopy

Fixation and immunolabeling using monoclonal antibody (mAb) 5E9 were as in Bowman and Turkewitz (2001) with two exceptions: the entire procedure was done at room temperature, and the primary incubation was with a 20% (vol/vol) solution of 5E9 hybridoma supernatant. Immunolabeling with 4D11 was as described previously (Bowman and Turkewitz, 2001). 4D11 and 5E9 were the gift of Marlo Nelson and Joseph Frankel (University of Iowa) and recognize p80 and *Grl3p*, respectively (Turkewitz and Kelly, 1992; Bowman *et al.*, 2005). For live cell microscopy, cells were immobilized in 1% (vol/vol) methyl cellulose (Carolina Biological, Burlington, NC). Samples were viewed under a Zeiss Axiocvert microscope interfaced with a Zeiss LSM 510 confocal laser system and software.

Flow Cytometry

Granule content of wild-type and Δ *GRL6* lines were analyzed by flow cytometry. For these experiments, cells (~1.5 × 10⁵/sample) from stationary phase (grown overnight, to 10⁶/ml) or overnight starved cultures were fixed with paraformaldehyde, permeabilized with Triton X-100, and immunostained in 1% bovine serum albumin in TBS, as described above. Cells were incubated with saturating concentrations (1:3 dilution of in vitro hybridoma culture supernatant, to a total volume of 0.4 ml) of either mAb 4D11 or 5E9. After washing, cells were suspended in 200 µl with 1% fluorescein isothiocyanate (FITC)-conjugated goat anti-mouse IgG (Molecular Probes, Eugene, OR), an amount that was also found empirically to be saturating. Negative controls had no primary antibody. Cells were analyzed on an LSR II flow cytometer (BD Biosciences, San Jose CA) using FACSDiVa software. Excitation was done using a 488-nm solid state Sapphire Laser (Coherent, Santa Clara, CA), and the collection filter was a 530/30 band pass filter.

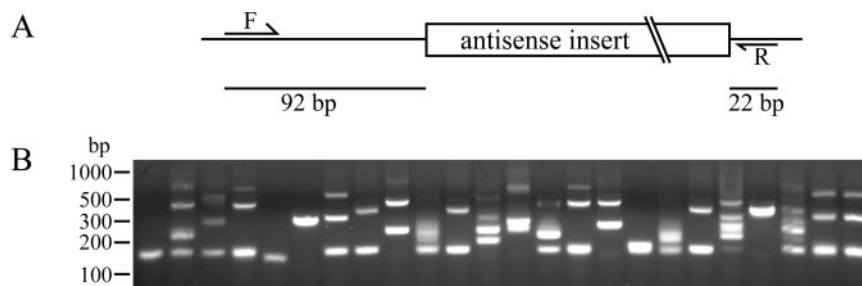
RNA Isolation, In Vitro Transcription, and Northern Blotting

CU428.1 RNA was isolated from exponentially growing cultures or from cells starved in a one-tenth dilution of Dryl's (1.7 mM sodium citrate, 1 mM NaH₂PO₄, 1.5 mM CaCl₂) supplemented with an additional 0.1 mM MgCl₂ and 0.5 mM CaCl₂ (DMC) for 6 h by using the RNeasy kit (QIAGEN, Valencia, CA). For in vitro transcription reactions, template open reading frames (ORFs) were each amplified from a cDNA library using the following primer pairs: *GRL1*, 5'-ATGAATAAGAAATATTAGTGTGCTTTT-3' and 5'-TCAGTTAATGAAGTCAATATTGGG-3'; *GRL2*, 5'-ATGCCCTTAACGT-TATTGTGAC-3' and 5'-TCAGAATCCACCAGAAGACTAGCA-3'; *GRL6*, 5'-ATGAAAATAATTATTATTTTTAGCCTC-3' and 5'-TCATTGGGATTA-TTCGCTGAT-3'; and *GRL7*, 5'-ATGAGAAAAGTCTTCGTTGCTT-3' and 5'-TCAAGCGCTTTCAGCACTT-3'. The PCR products were directionally cloned into pCRII (Invitrogen, Carlsbad, CA), and the resulting plasmids were linearized for run-off transcription with SP6 (sense) or T7 (antisense) RNA polymerase (Fermentas, Hanover, MD). These transcription products were ethanol precipitated and quantified for use as standards (sense) or as probe templates (antisense). RNA electrophoresis and Northern blotting were performed as per Farrell (1993). After electrophoresis on 1% agarose gels with formaldehyde, RNA was transferred and UV cross-linked to Magna (MSI, Westboro, MA) nylon membranes. Blots were visualized using a PhosphorImager (Amersham Biosciences, Sunnyvale, CA).

Construction of Antisense Libraries

Three antisense libraries were used in this screen. They were constructed using a PCR-based protocol, with one of two cDNA libraries as template. The first antisense library was constructed from the cDNA library described in Chilcoat *et al.* (2001). After digestion of the cDNA library with *SacI* and *XhoI* (to excise it from its pBluescriptvector backbone), we executed a single cycle of PCR with the primer 5'-TGCTAGCCACGGTCCGAGCGGGTACNNNNNN-3'. The six random nucleotides at the 3' end of this primer allowed it to anneal randomly within the library inserts, producing truncated copies with an added *KpnI* site. PCR conditions for this step were 95°C, 3:00; 15°C, 0:30; 70°C, 0:30; and 95°C, 2:00. The product of this reaction was diluted 10-fold and used as template with primers 5'-TGCTAGCCACGGTCC-

Figure 1. Whole cell PCR analysis of antisense transformants defective in capsule formation. (A) Schematic of the segment of the antisense library vector 5318Dnmod5 that flanks the antisense cloning site. Vector primers 5318f1 and 5318r2 (labeled F and R, respectively) were used to amplify antisense inserts with flanking vector sequence. (B) Representative 4% agarose gel of whole cell PCR reactions. Each lane represents the products of a single clone, the majority of which show more than one amplified insert.



CGAGCG-3' (contained within the above-mentioned primer) and 5'-biotin/ACCGCGTGGCGGCCGCTCTA-3' (containing a *NotI* site, and complementary to the vector backbone adjacent to the 5' ends of the cDNA inserts). PCR conditions for this step were 95°C, 2:00; 25 cycles of (95°C, 0:45; 53°C, 0:30; 70°C, 0:30); and 70°C, 10:00. After addition of fresh reagents and another cycle of PCR (95°C, 3:00; 50°C, 1:00; and 72°C, 3:00), the final PCR product was digested with *KpnI* before binding on a streptavidin plate (Pierce Chemical). After washing off unbound products, antisense inserts were eluted by digestion with *NotI*. After ethanol precipitation, the inserts were ligated into the ribosomal antisense vector 5318Dnmod (Chilcoat *et al.*, 2001). The cDNA library used as template for the second and third antisense libraries was constructed using the Creator SMART cDNA Library Construction Kit (BD Biosciences Clontech, Palo Alto, CA). Predigestion was with *SmaI* and *XhoI* or *EcoRI*, *XhoI*, *NotI*, *Clal*, and *Ascl* to excise the inserts from their pDNRLib vector backbone. PCR reactions were as described above, except that the biotinylated primer used was 5'-biotin/ATGCTCAGATCTATTGCATAGCGCCGCAATTCGCCATTACGGCCGGG-3'.

Transformation with Antisense Libraries and Screening

Mating pairs of B2086 and CU428.1 were transformed by electroporation using the ECM 600 (BTX, San Diego, CA) as described previously (Gaertig and Gorovsky, 1995). Initial drug selection was with 100 µg/ml paromomycin, added 16–24 h after transformation. After 3 d at 30°C, the transformants were screened to enrich for those with defects in exocytosis, as follows. After starvation overnight in DMC at 22°C, 50 ml of cells (at a density of 1×10^6 cells/ml) was stimulated with one-fourth volume of 0.1% Alcian Blue 8GX, added forcefully via syringe; after 30 s, an equal volume of 2% proteose peptone was added, and the cells were transferred to two 50-ml clear conical centrifuge tubes (Nalgene, Rochester, NY). The cells were pelleted in a clinical centrifuge for 1 min. Most of the supernatant was aspirated to leave 6–8 ml of fluid, in which the pelleted cells were gently resuspended. Over the next 5–10 min, encapsulated cells settled by gravity to the tube bottom, whereas free-swimming (exocytosis-deficient) cells migrated toward the air-water interface and concentrated at the meniscus. The latter were collected and transferred to 50 ml of fresh medium and grown for 8 h at 22°C, at which time the enrichment procedure was repeated. The free-swimming cells collected after this second step were diluted into fresh medium for distribution into 96-well plates (25 µl/well) at a density of ~30 single cells per plate. After 4 d at 30°C, the cells were starved by addition of 125 µl/well DMC and incubation at 30°C for an additional 4 d. Wells were then screened for the absence of capsules after stimulation with 25 µl of 0.1% Alcian Blue, followed by rescue with 25 µl of 2% proteose peptone. Initially, all encapsulation-deficient wells were confirmed by retesting, but this step was later omitted because of the negligible number of encapsulation-positive wells identified during rescreening, i.e., the assay results were highly reproducible.

Whole Cell PCR

Wells bearing encapsulation-deficient cells were replicated to master plates and grown to stationary phase. The antisense inserts harbored by the cells in each well were identified by whole cell PCR. Briefly, 50 µl of cells were mixed with 12.5 µl of K buffer (50 mM Tris-HCl, pH 8.8, 250 mM KCl, and 0.4% Nonidet P-40) and incubated for 1 h at 55°C and 10 min at 100°C. Then, 25 µl of this cell lysate was mixed with 25 µl of PCR mix (10 mM Tris-HCl, pH 8.8, 50 mM KCl, 0.08% Nonidet P-40, 2 mM MgCl₂, 2 mM of each nucleotide, 1 µM of the primers 5318f1 [5'-AAAAGTTCGATGAGTAAGGAAATG-3'] and 5318r2 [5'-CAATCTCAGGGTACGCGG-3'], and 3 U of *Taq*DNA polymerase [Fermentas]) and subjected to the following: 95°C, 3:00; 30 cycles of (94°C, 0:30; 55°C, 0:30; and 72°C, 1:00); and 72°C, 10:00. Products were visualized on 4% agarose gels, and those showing a single band were purified for sequencing. Products yielding antisense sequences of interest were digested with *KpnI* and *NotI* and ligated into the ribosomal antisense vector 5318Dnmod for retransformation of *Tetrahymena* by electroporation, as described above.

Expression of GFP-tagged Proteins

Grl2p-GFP and Grl6p-GFP were expressed in *Tetrahymena* from the vector pVGF.MTT, a modified version of pVGF.1 (Haddad *et al.*, 2002). pVGF.MTT

was created by replacing the ribosomal *RPL29* promoter in pVGF.1 (flanked by *NotI* and *PmeI* restriction sites) with the *MTT1* promoter (amplified from cDNA using primers 5'-CCGGTCACTTTTTTATTAGTAAAAAT-3' and 5'-CCGTTTAAACTATTTTAAAGTTTAGTATTAT-3') after replacing the *NotI* site with one for *BstEII*. The *GRL2*, *GRL6*, and *GRL7* coding sequences were amplified from cDNA using primer pairs 5'-AAGTTTAAACATGCGCTTA-CTGTTATTGTAC-3' and 5'-TTGTCAGCTGAAGAATCCACCAGAAC-TAGCACTT-3', 5'-ATGTTTAAACATGAAAAATAATTATTTTTTTAG-3' and 5'-TTAACAGCTGAATTGGGATTATTCGTCTGATC-3', and 5'-ACGTTTAAACATGAGAAAAGTCTTCGTTGCTT-3' and 5'-TATCAGCTGAAAG-CGCTTTCAGCACTTCC-3', respectively; these pairs provide restriction sites for blunt ligation into pVGF.MTT at its *PmeI* site. The second primer of each pair removes the stop codon from the end of the coding sequence, allowing for insertion in frame with an enhanced GFP tag (BD Biosciences Clontech) in the vector. Correct ligation was verified by direct sequencing. After transformation into *Tetrahymena*, protein expression was induced by growth in 0.2% yeast extract, 0.009% ferric EDTA with 0.1 µg/ml CdCl₂ for 24 h at 30°C. Grl1p-GFP was expressed from the *ncvB* vector (Bowman *et al.*, 2005), which results in the expression of protein from the endogenous chromosomal *MTT1* locus. The Grl1p-GFP coding sequence was produced by creating the GFP fusion protein in pVGF.MTT (as above, using primers 5'-GTTTAAACAT-GAATAAGAAATTATTA-3' and 5'-TTGTCAGCTGAAGTTAATGAAGTC-AATATTGG-3'), and shuttling this fusion into *ncvB* using the flanking *PmeI* and *ApaI* restriction sites. The Grl1p-GFP coding sequence was produced by shuttling the *IGR1* ORF from the pVGF.1 vector (Haddad *et al.*, 2002) into the pVGF.MTT vector (using *PmeI* and *XhoI* restriction sites), followed by the insertion of the GFP tag and transfer into *ncvB*, as described above. Grl1p-GFP expression was induced by growth in SPP with 2 µg/ml CdCl₂ for 6–8 h at 30°C.

High Level Expression of GRL1

The *GRL1* coding sequence was amplified from cDNA using the primers 5'-GTTTAAACATGAATAAGAAATTATTA-3' and 5'-CTCGAGTCAGTTA-ATGAAGTCAAT-3', which provide restriction sites for insertion into pVGF.MTT between the *PmeI* and *XhoI* sites. This ligation step removes the GFP sequence from the vector, resulting in the expression of full-length untagged *GRL1*. Protein expression was induced by growth in SPP with up to 3 µg/ml CdCl₂ for 4–5 h at 30°C.

Expression of GRL1-6xHis

The endogenous *GRL1* coding sequence was replaced with *GRL1*-6xHis by modifying a vector used by Bradshaw *et al.* (2003) to replace the endogenous *GRL1* gene with genes that contain altered *GRL1* coding sequences. Starting with a template vector that encodes the wild-type Grl1p sequence, the primers 5'-CACCACCACCACCACCCTGAAAAATGATGTGATTT-3' and 5'-GTTAATGAAGTCAATATTGG-3' (MWG, High Point, NC) were used to amplify the vector by inverse PCR. The amplified product was blunted with T4 DNA polymerase and then digested with *DpnI* to destroy the template before self-ligation (New England Biolabs, Beverly, MA). The modified coding sequence (full length *GRL1* plus six histidine codons placed immediately upstream of the stop codon) was confirmed by sequencing, and the construct was used for biolistic transformation of CU428.1.

Purification of proGrl1p-His Complexes

Purification followed Bowman *et al.* (2005) except that the lysis, wash, and elution buffers did not contain urea or guanidine.

Production of Polyclonal Anti-Grl4p Antibodies

To obtain immunogen for the production of anti-Grl4p antibodies, secretory granule contents were purified from wild-type cells (Turkewitz *et al.*, 2000). Approximately 1 mg of this material was resolved on a 20% polyacrylamide gel in SDS and then stained with Coomassie Blue. Guided by previous identification of polypeptides in such samples (Verbsky and Turkewitz, 1998), Grl4p was excised with a scalpel. Rabbit antiserum against this band was then produced commercially (Zymed Laboratories, South San Francisco, CA).

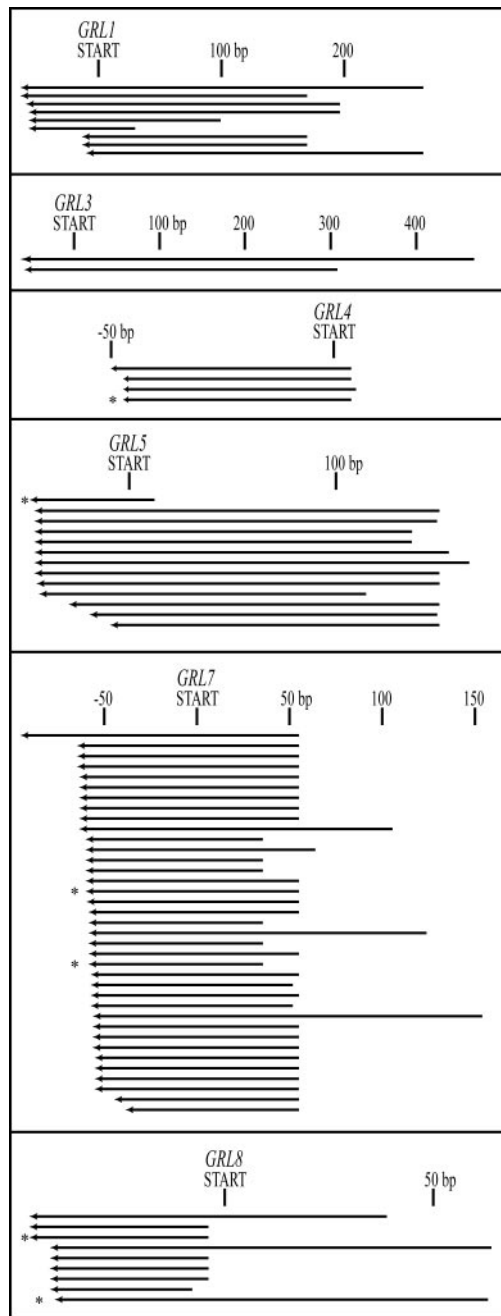


Figure 2. Schematic of all GRL antisense sequences isolated from exocytosis-deficient transformants. Sequences, which are represented as arrows, fall into six groups that correspond to the known GRLs. Nucleotide positions indicated at the top of each group are relative to the start codon of the indicated GRL. In cases where identical sequences were obtained from multiple clones arising from a single transformation, only a single arrow is shown. Six sequences (marked with an asterisk) were used to transform wild-type cells, and each of these antisense sequences conferred an exocytosis-deficient phenotype. All antisense sequences contain a portion of the 5' untranslated region of their respective genes.

Exocytosis Testing of Δ GRL Strains

Strains were tested for Alcian Blue-induced capsule formation by using cultures starved overnight in DMC and for dibucaine-induced flocculent release by using stationary cultures ($0.8\text{--}1 \times 10^6$ cells/ml in SPP medium) as described previously (Turkewitz and Kelly, 1992; Melia *et al.*, 1998). To

quantify dibucaine-stimulated release from Δ GRL6 cells relative to wild-type, 6×10^6 cells were suspended in 1 ml of 10 mM Na-HEPES, pH 7.0, 0.5 mM CaCl_2 , and stimulated for 15 s by addition of 110 μl of 25 mM dibucaine. Cells were then diluted with buffer to 15 ml and pelleted for 5 min at $300 \times g$. The released granule contents, which form a distinct flocculent layer above the cell pellet, were removed with a transfer pipette and transferred to a graduated conical tube for repelleting and volume measurement. Protein concentrations in the flocculent layer were measured using the Pierce protein assay.

Analysis of Functionality through Evolutionary Constraint

The translations of the sequences were first aligned using ClustalW using default parameters. Afterward the codons were mapped directly onto the peptide alignments to produce a multiple alignment with gaps in multiples of three. For estimating rates of evolution, an unrooted phylogeny for the three genes was assumed. The substitution rates at amino acid changing sites (K_A) and at synonymous sites (K_S) were calculated using the codeml software (Yang 1997). K_A is the ratio of number of nucleotide substitutions that result in an amino acid change to the total possible number of amino acid changing nucleotide substitutions. K_S is a similar ratio corresponding to synonymous changes within codons. The ratio K_A/K_S (also called ω) reflects the nature evolutionary constraint between sequences. Because silent substitutions do not affect the peptide, the K_S ratio is used as a neutral standard. If $K_A = K_S$ ($\omega = 1$), this indicates a lack of constraint at the amino acid level. If, however, $K_A < K_S$ ($\omega < 1$), then the rate of protein evolution is constrained, indicating selection against amino acid substitution and implying protein functionality. Finally, if $K_A > K_S$ ($\omega > 1$), then protein evolution is accelerated, indicating natural selection for amino acid substitution. Evolutionary constraint was evaluated by testing four separate models of protein evolution. In the first model (H_0), the rates of all branches were estimated from the data. In the remaining three models, ω in the branch leading to each sequence was fixed at a value of 1 (neutrality), whereas the other branches were estimated. The models are described as follows: H_0) Estimate ω for all branches; H_1) Set ω for GRL5 = 1, and estimate the others; H_2) Set ω for GRL9 = 1, and estimate the others; and H_3) Set ω for GRL10 = 1, and estimate the others.

To evaluate the probability that a given sequence differed from the neutral rate of $\omega = 1$, a likelihood ratio test (Yang, 1998) between H_0 and each model was conducted as follows. The χ^2 statistic is calculated as

$$\chi^2 = 2(\ln(L_{H_0}) - \ln(L_{H_i})) \quad (1)$$

where L represents the likelihood of the model H_1 . The χ^2 statistic is χ^2 distributed with 1 degree of freedom.

RESULTS

Screening for Antisense Ribosomes That Confer Exocytosis Defects

To identify genes required for regulated exocytosis of secretory granules in *T. thermophila*, we transformed cells with both existing as well as new libraries of antisense ribosomes. We screened transformants to identify the subset with defects in exocytosis, as judged by the inability to form capsules when stimulated with the secretagogue Alcian Blue. Such cells were obtained first by physical enrichment and then by visual screening of individual clones in 96-well plates. Clones that failed to undergo visible exocytosis when challenged with Alcian Blue were expanded, and the antisense inserts were then amplified by whole cell PCR using primers directed against the insert flanking sites at the rDNA locus. As can be seen in a representative agarose gel, multiple PCR products were obtained for many transformant lines (Figure 1). These were due to multiple antisense inserts within individual cells, rather than to nonclonality among the transformant lines, because we obtained the same result when single cells were again isolated and clonally expanded (our unpublished data). For practical purposes, we focused on the subset of cells seeming to have a single major insert.

We obtained sequences of 304 antisense inserts associated with strong defects in exocytosis in the primary screen. From these sequences, we then identified the corresponding genes by querying the expressed sequence tag (EST) database, in which a large fraction of entries include sequence from the 5' untranslated region. Of these 304, 237 had previously been

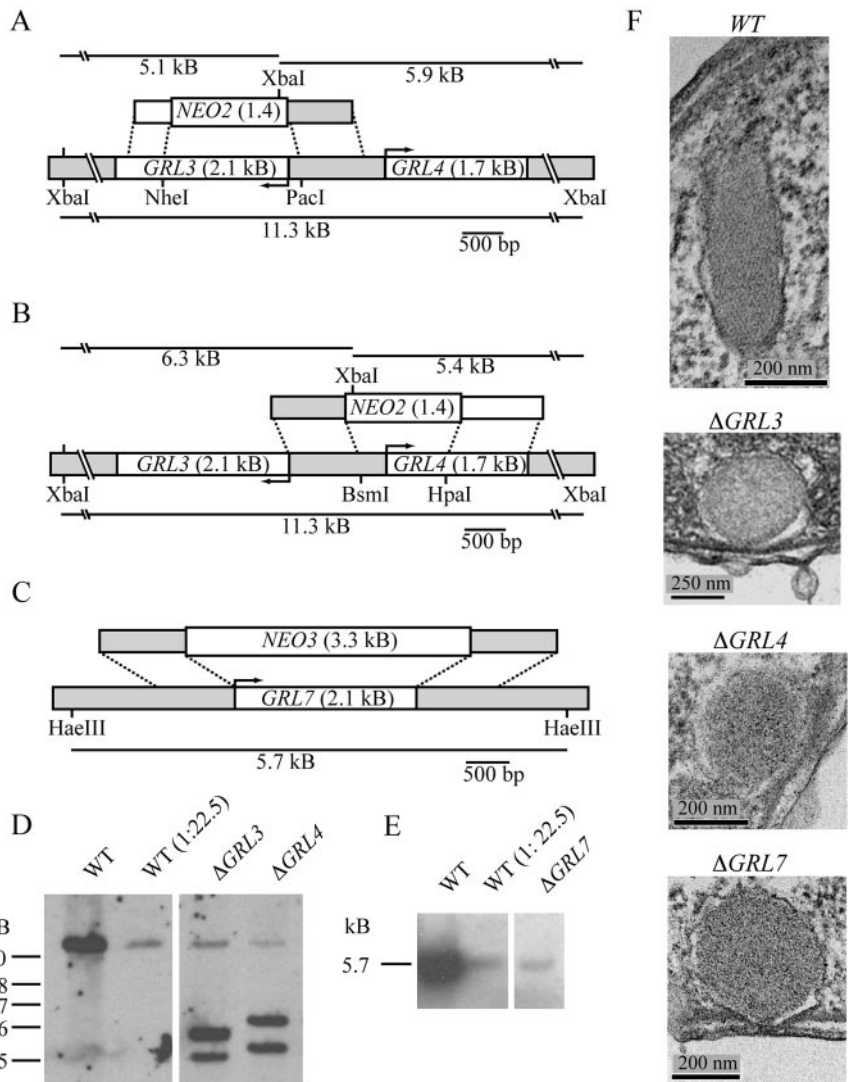


Figure 3. Disruption of *GRL3*, *GRL4*, and *GRL7* through homologous recombination. (A) *GRL3/4* genomic locus, showing the replacement by the NEO2 cassette of the first 508 aa of the *GRL3* ORF. In A, B, and C, noncoding regions are shown in gray. (B) *GRL3/4* locus, showing the replacement by the NEO2 cassette of the first 242 aa of the *GRL4* ORF. (C) *GRL7* genomic locus, showing replacement by the MTT-NEO cassette of the entire *GRL7* ORF. (D) Southern blot of genomic DNA from *GRL3* and *GRL4* knockout lines, with probes generated from the cDNAs of the respective genes as described in *Materials and Methods*. An additional *XbaI* site in the NEO2 cassette results in hybridization of the probe to two smaller fragments; the remaining material at the size of the wild-type locus is transcriptionally silent micro-nuclear DNA, present 2N relative to the 45N of the transcriptionally active macronuclear DNA (a 22.5-fold decrease in signal, as shown). (E) Southern blot of a *GRL7* knockout line, using a probe generated from the *GRL7* cDNA. In this case, none of the *GRL7* ORF remains for hybridization with the probe; the remaining signal is from detection of micro-nuclear DNA. (F) Electron micrographs of wild-type, Δ *GRL3*, Δ *GRL4*, and Δ *GRL7* granules, showing the aberrant morphology and lack of a crystalline lattice in the knockout lines. Bars, 0.2, 0.25, 0.2, and 0.2 μ m, respectively.

identified in *T. thermophila*, and 67 were novel. Among the former were all six of the known *GRL* family (*GRL1*, 3, 4, 5, and 7, and *NDC1/GRL8*, and multiple independent inserts were obtained corresponding to each family member; Figure 2). For the sake of simplicity, we henceforth refer to *NDC1* as *GRL8*. In fact, inserts corresponding to *GRL* genes comprised 181 of these inserts (Figure 2). We confirmed the significance of a subset of these inserts by reinserting them into the empty rDNA vector and generating new transformants for testing. In all cases, inserts corresponding to *GRL* genes regenerated exocytosis-deficient transformants. The remaining 56 previously identified genes all fell into the class of “housekeeping” genes, particularly corresponding to ribosomal proteins, whose suppression would be predicted to impair cell viability. Because housekeeping genes were unlikely to have roles specific for granule synthesis, they were not further examined.

To begin analyzing the set of novel genes, we first tested the ability of the inserts to regenerate the exocytosis deficiencies, as described above. However, in contrast to the *GRL* gene inserts, in no case did retransformation regenerate the exocytosis deficiency. In such cases, the primary transformants may have harbored one or more additional rDNA inserts, not detected by whole cell PCR, that were responsi-

ble for the deficiencies. Previous work has demonstrated that an antisense ribosome constituting just a small minority of the total ribosome population in a given cell can produce a null or hypomorphic phenotype (Sweeney *et al.*, 1996). Alternatively, the deficiencies may have been due to mutations unrelated to the rDNA locus, induced as a result of the transformation process. The genes corresponding to these inserts were not analyzed further.

Testing *GRL* Function by Individual Gene Disruption

Although this functional screen did not succeed in identifying new genes involved in regulated secretion, the results strongly suggested that each of the *GRL* gene products, previously identified by isolation of DCG contents, plays an essential, nonredundant role in regulated exocytosis. To test this directly and to evaluate the function of individual *Grl* proteins, we disrupted each of three *GRL* genes (*GRL3*, *GRL4*, and *GRL7*) in independent cell lines (Figure 3). We did not target *GRL5* for disruption because Southern blotting indicated that multiple gene copies might be present. This issue was clarified when the *T. thermophila* genomic sequence became available and is discussed in a later section. As expected, the Δ *GRL3*, Δ *GRL4*, and Δ *GRL7* lines were

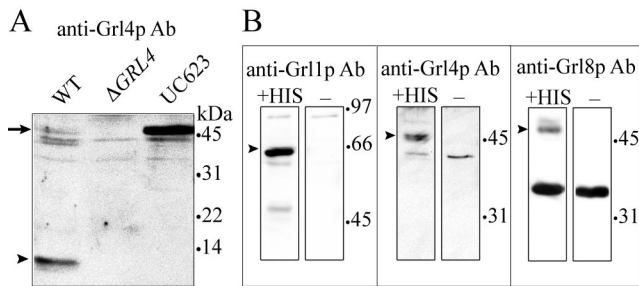


Figure 4. Affinity chromatography of proGrl1p complexes. (A) Identification of proGrl4p and Grl4p by Western blotting. Whole cell lysates of wild-type, $\Delta GRL4$, and UC623 cells were resolved on a 17.5% gel and probed with the anti-Grl4p antibody on Western blots. Compared with $\Delta GRL4$, the wild-type lane has two extra bands. The more abundant species, at 12 kDa, corresponds to the mature product generated from the amino-terminal half of proGrl4p (Verbsky and Turkewitz, 1998), whereas the lighter band at 47 kDa corresponds to proGrl4p. Consistent with these assignments, the latter is much more abundant, and the former absent, in a lysate from the UC623 mutant line that accumulates unprocessed proGrl proteins (Bowman *et al.*, 2005). (B) proGrl4p and proGrl8p physically interact with proGrl1p. In wild-type cells, the endogenous *GRL1* gene was replaced by a construct that adds a C-terminal 6His-tag to the *GRL1* open reading frame and maintains expression from the endogenous promoter. Transformed cells were lysed as described in *Materials and Methods*, and proGrl1p-6His-containing complexes were purified from a high speed supernatant by affinity chromatography. The purified material (+His) was run on a 12.5% gel and probed with the anti-Grl1p, anti-Grl4p, and anti-Grl8p antibodies by Western blot. The control lanes (–) contain material purified from wild-type cells that were not transformed with the His-tag construct and contain material that was nonspecifically bound by the column. Specifically bound species, corresponding to Grl proproteins, are indicated by arrowheads. The electrophoretic positions of molecular weight standards are indicated on the right of each panel.

each completely defective in Alcian Blue-stimulated capsule formation (our unpublished data; Figure 11). The deficiencies were due to defects in DCG synthesis and specifically in the assembly of the core structure. As revealed by electron microscopy, each of the ΔGRL lines accumulated aberrant DCGs that differed from the wild type in shape, being spherical rather than elongated (Figure 3F). In addition, the spherical granules lacked any visibly ordered core structure. There were no discernible differences between the granules formed in these different strains; moreover, we also found similar granules in a double-disruption $\Delta GRL3$, $\Delta GRL4$ cell line (our unpublished data). At this level of analysis, the granules in strains lacking *GRL3*, *GRL4*, or *GRL7* seemed structurally and functionally identical to those previously characterized in $\Delta GRL1$ or $\Delta GRL8$ cells (Chilcoat *et al.*, 1996; Chilcoat *et al.*, 2001). These results differed markedly from those in *Paramecium*, in which distinct granule assembly defects were induced by silencing of specific *tmp* families (Vayssie *et al.*, 2001). Instead, our results suggested that the *Tetrahymena* Grl proteins all play similar roles during core formation. To account for these results, we hypothesized that each protein is present throughout the elongated lattice found in wild-type cells. One possibility is that each contributes to a Grl hetero-oligomeric complex, which could function as an assembly subunit.

In Vitro Evidence for proGrl Hetero-oligomeric Complexes

To determine whether such hetero-oligomers exist, we began with a biochemical approach. Attempts to dissociate

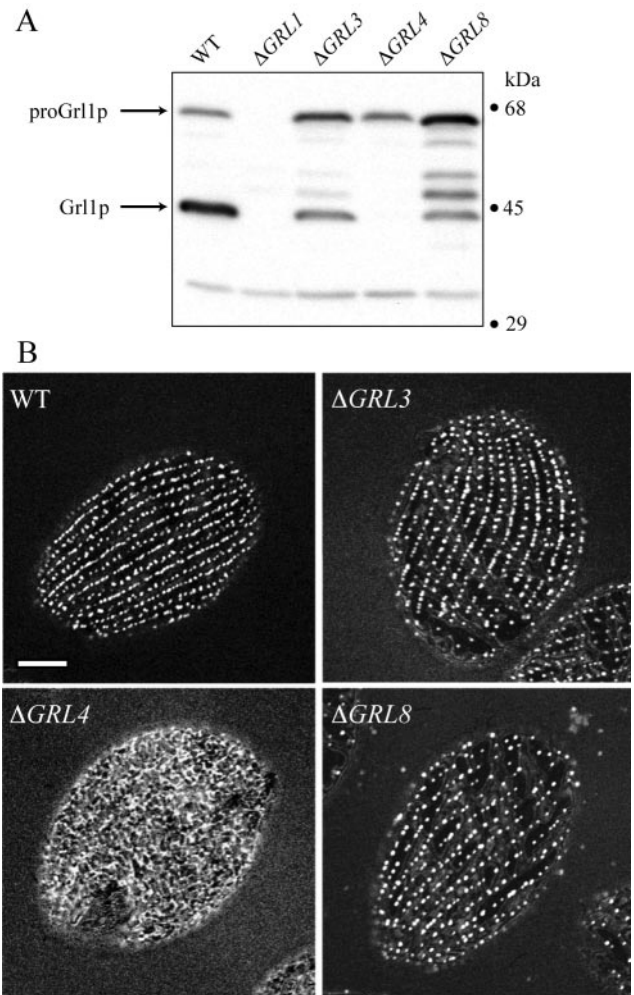


Figure 5. *GRL4* is required for proGrl1p exit from the endoplasmic reticulum. (A) *GRL4* is required for proGrl1p processing. Whole cell lysates of wild-type cells and the indicated ΔGRL strains were resolved on a 12.5% gel and probed with the anti-Grl1p antibody by Western blotting. The disruption of *GRL3* or *GRL8* has a partial inhibitory affect on the accumulation of processed Grl1p, whereas the disruption of *GRL4* results in complete inhibition of proGrl1p processing. The ladder of intermediate bands in the $\Delta GRL3$ and $\Delta GRL8$ samples may be accounted for by weak cross-reactivity of the anti-Grl1p antibody for other Grl proproteins. The relative abundance of the proGrl and mature Grl species cannot be compared in this experiment, because the former seems to be more immunoreactive under Western blotting conditions (our unpublished data). (B) *GRL1*-GFP was expressed in wild-type cells and the indicated ΔGRL strains, and GFP localization was determined by confocal microscopy on live cells. Each confocal image shows the top surface of a single cell. In $\Delta GRL4$ cells, the proGrl1p-GFP resides in a subplasma membrane reticulum. In all other strains, the fluorescent proteins localize to docked granules. Bars, 10 μ m.

mature granule cores into putative subunits were foiled by the striking stability of the assembled lattice under all but strongly denaturing conditions (our unpublished data). On the other hand, before proteolytic processing and core assembly, the Grl proteins are fully soluble (Turkewitz *et al.*, 1991). To ask whether Grl proproteins assemble as hetero-oligomers, we engineered *GRL1* with a carboxy-terminal hexahistidine extension. This was recombined at the native *GRL1* locus as a gene replacement, to achieve a wild-type

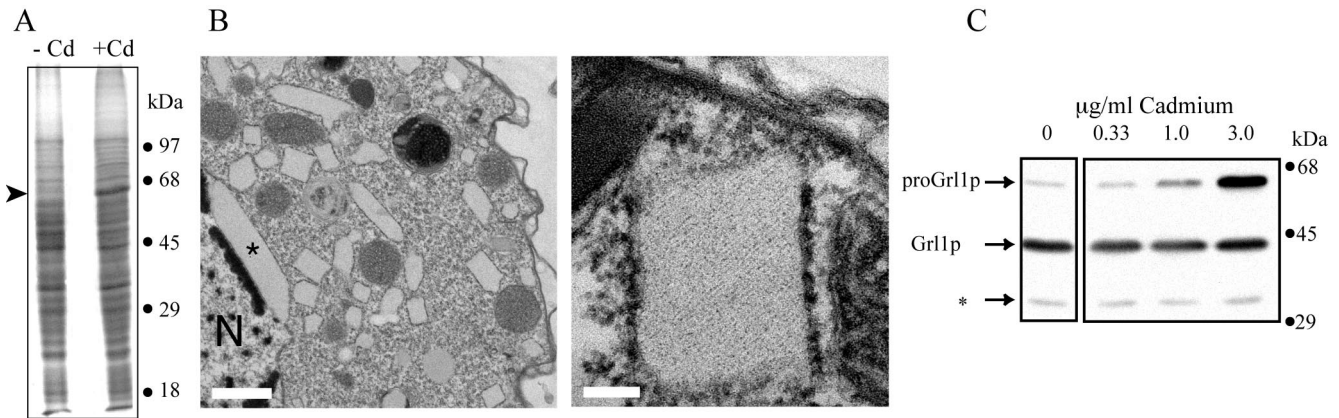


Figure 6. Overexpression of *GRL1* results in the retention and crystallization of proGrl1p in the ER. (A) The accumulated proGrl1p in cadmium-induced cells constitutes a significant percentage of total cellular protein. Cells were transformed with the cadmium-inducible *GRL1* expression vector. Whole cell lysates from either uninduced or 3.0 µg/ml cadmium-stimulated cells were analyzed by Coomassie Blue staining (12.5% polyacrylamide gel). A pronounced band at 60 kDa, corresponding to proGrl1p, is exclusively present in the induced sample (arrow). (B) ProGrl1p crystallizes in the ER. Cells overexpressing proGrl1p, induced as in A, were fixed and prepared for electron microscopy. Left, at low magnifications, a large number of straight-edged inclusions are visible. The asterisk indicates an inclusion that has formed in the envelope of endoplasmic reticulum that separates the nucleus (labeled N) from the cytosol. Bar, 1 µm. Right, high-magnification view reveals striated patterning in the inclusion bodies, indicating that the contents are crystalline. Docked ribosomes can be seen along the cytoplasmic membrane surface. Bar, 0.2 µm. (C) The extent of proGrl1p processing is independent of proGrl1p expression level. Expression of *GRL1* from the inducible *GRL1* expression vector was induced with the indicated cadmium concentrations for 6 h, and whole cell lysates of these cultures were resolved on a 12.5% gel and probed by Western blotting with anti-Grl1p antibody. The positions of proGrl1p and Grl1p are indicated. A cross-reactive band, marked by the asterisk, serves as a loading control.

pattern and level of expression. ProGrl1p-6His was isolated from nondenaturing detergent cell lysates by nickel affinity chromatography, and antibodies against other Grl proteins were used to ask whether these coeluted with proGrl1p-6His. Mature processed Grl1p is entirely insoluble under these conditions, and was therefore discarded before the chromatography step. Western blotting, after SDS-PAGE and transfer to nitrocellulose, revealed that at least two other proGrl proteins were bound to the nickel-Sepharose, in a manner that depended on the presence of proGrl1p-6His (Figure 4). Although these data do not establish whether one or more of these proteins directly contacts proGrl1p or whether such contacts are specific, they are consistent with assembly of a set of Grl proproteins as an early step in core formation. Because we do not possess antibodies against the remaining Grl proteins, we could not determine whether these were also present.

In Vivo Evidence for Hetero-oligomer Formation

To understand the *in vivo* significance of such oligomers, we analyzed Grl proteins in a subset of the *GRL* null lines described previously. The logic of these experiments was that specific oligomer formation, if it occurred at the level of the ER, could be a prerequisite for ER exit. This has been observed for multimeric complexes in many other systems, including at least one complex targeted to secretory granules (Chanat *et al.*, 1999). We therefore asked whether the absence of other Grl proteins blocks ER exit of proGrl1p. As a first measure, we assessed the extent of proGrl1p processing, a step that occurs in a post-*trans*-Golgi network (TGN) compartment and which therefore requires exit from the ER. The processing of proGrl1p was significantly inhibited in $\Delta GRL4$ cells (Figure 5A). That this reflected a specific interaction between proGrl1p and proGrl4p was supported by the observation that only a partial inhibition was seen in $\Delta GRL3$ and $\Delta GRL8$ cells. The results suggested that proGrl1p, when expressed in the absence of proGrl4p, failed to reach the

post-TGN processing compartment due to its retention in the ER. To assess this more directly, we expressed a GFP-tagged variant of *GRL1* in wild-type, $\Delta GRL3$, $\Delta GRL4$, and $\Delta GRL8$ cells. In wild-type cells, the protein localized as expected to the docked DCGs (Figure 5B). In $\Delta GRL4$ cells, on the other hand, Grl1p-GFP was found primarily in a subcortical reticular pattern, distinct from the punctate pattern of docked DCGs. This reticular pattern is likely to reflect the cortical endoplasmic reticulum but also may overlap with alveoli, which are flattened cisternae underlying the plasma membrane (Frankel, 2000). Alveoli are involved in calcium-based signaling and may represent a specialized ER subcompartment. We observed identical patterns in cells transformed to express GFP (with an N-terminal signal sequence), fused at the C terminus to carboxy-terminal tetrapeptides that confer ER localization in other species (KDEL or HDEL) (our unpublished data) (Andres *et al.*, 1991). This localization depended upon the ER retention signal, because signal sequence GFP, without any ER-retention signal, localizes to small cytoplasmic vesicles in these cells or is found in the medium (Haddad *et al.*, 2002; Bowman *et al.*, 2005). Importantly, mislocalization of proGrl1p-GFP to the cortical reticulum in $\Delta GRL4$ cells was specific, because Grl1p-GFP expressed in $\Delta GRL3$ and $\Delta GRL8$ cells accumulated primarily in the DCGs. Unlike in wild-type cells, $\Delta GRL3$ and $\Delta GRL8$ cells also showed a low level of proGrl1p-GFP labeling of non-DCG structures, consistent with the partial inhibition of processing (Figure 5B).

GRL1 Overexpression Leads to ER Accumulation

These results suggested that proGrl1p and proGrl4p associate at the level of the ER, as a prerequisite to ER exit. This may regulate the stoichiometry of subunit assembly in the multicomponent lattice. A prediction was that overexpression of *GRL1* would lead to its partial retention in the ER, because the amount of proGrl4p or other potential binding partners would be limiting under such circumstances. To

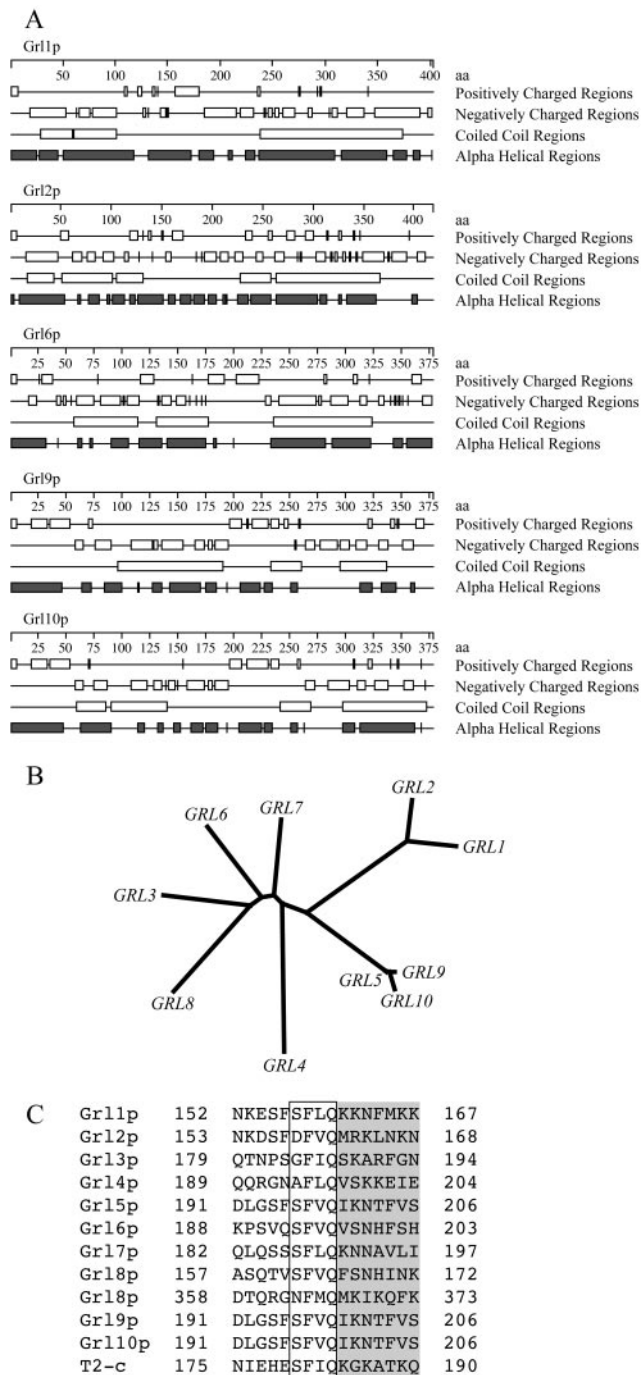


Figure 7. Four new members of the *GRL* family. (A) Predicted structural features of Gr11p and of the four newly identified family members. (B) A phylogenetic tree displaying the evolutionary relationship between the Gr11ps. After aligning the protein sequences using the ClustalW algorithm, a phylogenetic tree was calculated using the maximum likelihood algorithm in the PHYLIP software suite. The branching pattern reveals two clusters of relatively closely-related paralogs (*GRL1* and 2, and *GRL5*, 9, and 10) within a tree that is otherwise made up of deep lineages. (C) Alignment of the Gr11ps and a member of the *Paramecium* tmpps, illustrating a tetrapeptide motif (boxed) that lies amino-terminal to the central basic stretch and to the carboxy-terminal basic stretch of Gr18p (shown in gray). With its substitution of a charged residue (Asp) within the motif, Gr12p deviates from the pattern established by the other family members.

test this, we expressed *GRL1* from a multicopy rDNA-based vector, under the control of the *MTT1* promoter. Gr11p accumulated in the cells in the proprotein form, at a level so high that it was visible as a prominent Coomassie Blue-staining band after SDS-PAGE of whole cell lysates (Figure 6A). Analysis of these cells by thin sectioning and electron microscopy revealed that the cytoplasm contained abundant ER filled with a visible aggregate, organized in some regions as a geometric lattice (Figure 6B). This crystallization was probably widespread, because many ER lumina were distended in distinctly angular shapes. Such distended ER is not seen in wild-type cells. Interestingly, cells overexpressing *GRL1* also had a normal complement of docked DCGs with wild-type morphology, suggesting that the endogenous level of proGr11p still exits the ER even while most of the proGr11p is retained (our unpublished data). Consistent with this, Western blotting of whole cell lysates, derived from cultures induced over a range of cadmium concentrations, showed that a constant amount of mature Gr11p was generated, irrespective of the *GRL1* expression level (Figure 6C).

It is also noteworthy that the proGr11p in such overexpressing cells did not seem aggregated by biochemical criteria. When cells were solubilized in non-denaturing detergent (1% Triton X-100), essentially all of proGr11p was soluble ($350,000 \times g$; 20 min) (our unpublished data). These results suggest that ER retention of proGr11p is not due to misfolding.

Genome Analysis Reveals Four Novel *GRL* Genes

Previous biochemical analysis as well as the functional screen reported here converged on a set of six *GRL* genes. In particular, the results of the latter suggest that no other genes play essential roles in granule assembly. However, genes with redundant functions would have been invisible. The same may be true for genes with nonredundant functions that are transcribed at a low level, because representation in the antisense libraries depends in part on relative mRNA abundance. We took advantage of the recent completion of the sequencing of the *T. thermophila* macronuclear genome, in addition to establishment of an EST database, to ask whether these six genes represent the entire *GRL* family. Homology searches with each of the six genes revealed the likely existence of four novel related genes in the macronuclear genome, which we have named *GRL2*, 6, 9, and 10 (Figure 7A). The relationship between the *GRLs* is shown in Figure 7B. The predicted new family members all bear characteristic Gr1 protein features, including their overall length, highly acidic character, and a wealth of predicted short α -helical coiled coils. The extent of amino acid identity between the six previously identified *GRL* genes is low, on the order of 20% (Verbsky and Turkewitz, 1998). This is also true for *GRL6*, but the other three newly detected *GRL* genes show a pattern indicating a different evolutionary history. *GRL9* and 10 are very closely related ($\geq 85\%$ identity) to *GRL5*, and their hybridization with a *GRL5* probe can account for the Southern blotting results mentioned previously. *GRL2* is most closely related ($>40\%$ identity) to *GRL1*. The genes seem to represent relatively recent duplications in an otherwise deeply branched phylogeny. Gr12p is unusual in having a nonconservative substitution within a four-amino acid motif that is the most highly conserved 1° structural feature in the Gr1/tmp family (Figure 7C) (Verbsky and Turkewitz, 1998).

The fact that these four hypothetical genes eluded previous detection suggested that some of their products might have roles distinct from the six established members. Func-

tional analysis was confined to *GRL2* and *6*, because the similarity of *GRLs* 5, 9, and 10 made it challenging to target those genes individually. *GRL9* and 10 are likely to be transcribed at relatively low levels, because many independent *GRL5* clones, but no *GRL9* or 10 clones, were identified in the EST library (all EST sequences available through standard public databases). However, neither *GRL9* nor 10 seems to be a pseudogene, based on direct and indirect evidence. The *GRL9* product was unambiguously detected in mass spectrometric analysis of isolated granules (our unpublished data). The argument for *GRL10* is based on analysis presented below, indicating that this gene is evolving under natural selection for amino acid substitution. Because pseudogenes are expected to evolve neutrally, this is evidence against *GRL10* being a pseudogene.

To test for the presence or absence of functional constraint during evolution of *GRL5*, *GRL9*, and *GRL10*, we measured the divergence between the sequences. Some nucleotide substitutions in a codon do not change the peptide sequence (synonymous substitutions), whereas others result in the substitution of one amino acid residue for another (replacement substitutions). The ratio of synonymous substitutions to total number of synonymous sites is called K_S , whereas the ratio for replacement substitutions is called K_A . Under the assumption that synonymous substitutions are invisible to natural selection and thus represent the mutation rate in the absence of selection, the ratio of K_A to K_S , or ω , measures the selective constraint on amino acid substitutions in a sequence. Table 1 shows the results of testing the rates of evolution on the unrooted phylogeny between *GRL5*, *GRL9*, and *GRL10*. These results indicate that the rates of nonsynonymous substitution for *GRL5* and *GRL9* do not differ significantly from the rates of synonymous substitution, be-

Table 1. Measurement of evolutionary divergence between *GRL5*, *GRL9*, and *GRL10*

	K_A	K_S	ω	χ^2	P
<i>GRL5</i>	0.0538	0.0816	0.66	1.686	0.194
<i>GRL9</i>	0.02813	0.0483	0.58	1.5122	0.219
<i>GRL10</i>	0.13429	0.0485	2.77	9.9041	0.00165

cause the ratio ω does not differ significantly from 1. However, for *GRL10* in particular the rate of replacement substitution is significantly elevated with respect to synonymous substitution, because its value of ω is significantly greater than 1. This suggests that *GRL10* is not evolving as would be expected for a pseudogene, i.e., neutrally.

In Vivo Analysis of *GRL2* and *GRL6*

GRL2 was present as a single clone in the EST library, and both *GRL2* and *6* could be amplified by PCR as full-length copies from cDNA libraries, indicating that these genes are transcribed. As shown by Northern blotting, however, the mRNAs are present at levels much lower than those of the previously described *GRL* genes (Figure 8). The regulation of expression also seems to be different, because *GRL1* and *7*, but not *2* and *6*, show greater accumulation (as a fraction of total mRNA) in starvation versus growth conditions. To characterize *GRL2* and *6*, we first asked whether the gene products localize to DCGs by engineering them as GFP-tagged copies. As shown in Figure 9, expression of either *Grl2p*-GFP or *Grl6p*-GFP from the *MTT1* promoter produced a fluorescent array of cortical puncta, indicating that

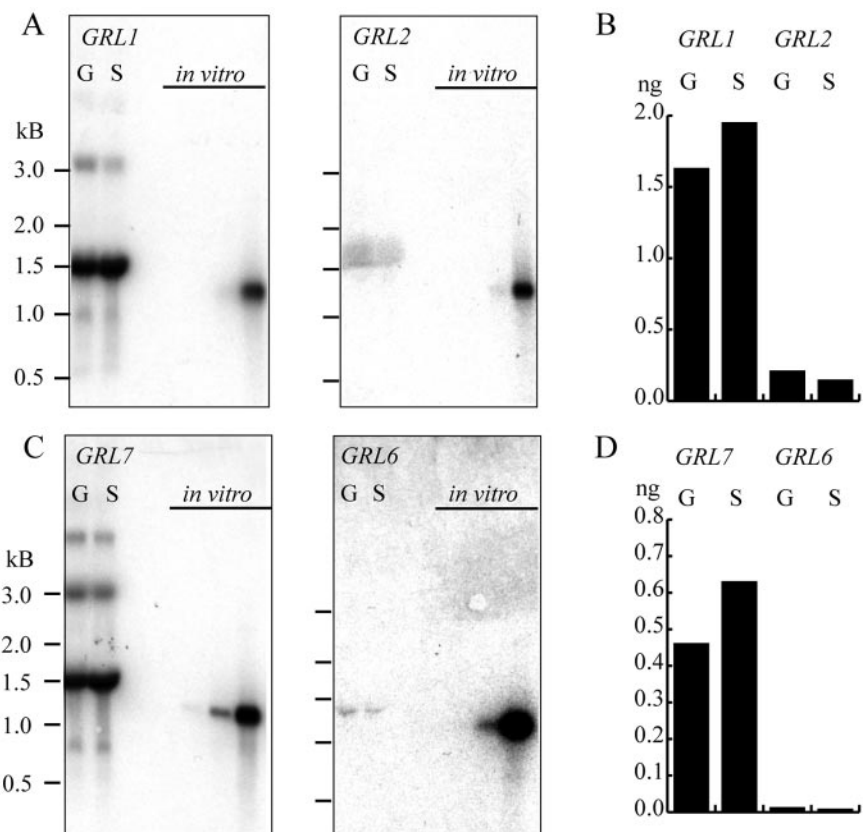


Figure 8. Northern analysis of two novel *GRLs*. (A) Cellular RNA (9.4 μ g) from growing (G) and starved (S) wild-type cells, labeled with a probe generated from the *GRL1* (left blot) or *GRL2* (right blot) open reading frames. At right on each blot is *GRL1* (left blot) or *GRL2* (right blot) RNA from *in vitro* transcription reactions, in loadings of 1 pg, 10 pg, 100 pg, and 1 ng. (B) For each of the blots in A, the 100-pg and 1-ng *in vitro* products were used to construct a linear scale. These scales were used to quantitate the amount of *GRL1* and *GRL2* RNA in G and S cells. (C) Northern blots as for A, probing for *GRL7* and *GRL6*. (D) Analysis of the *GRL7* and *GRL6* blots as in B.

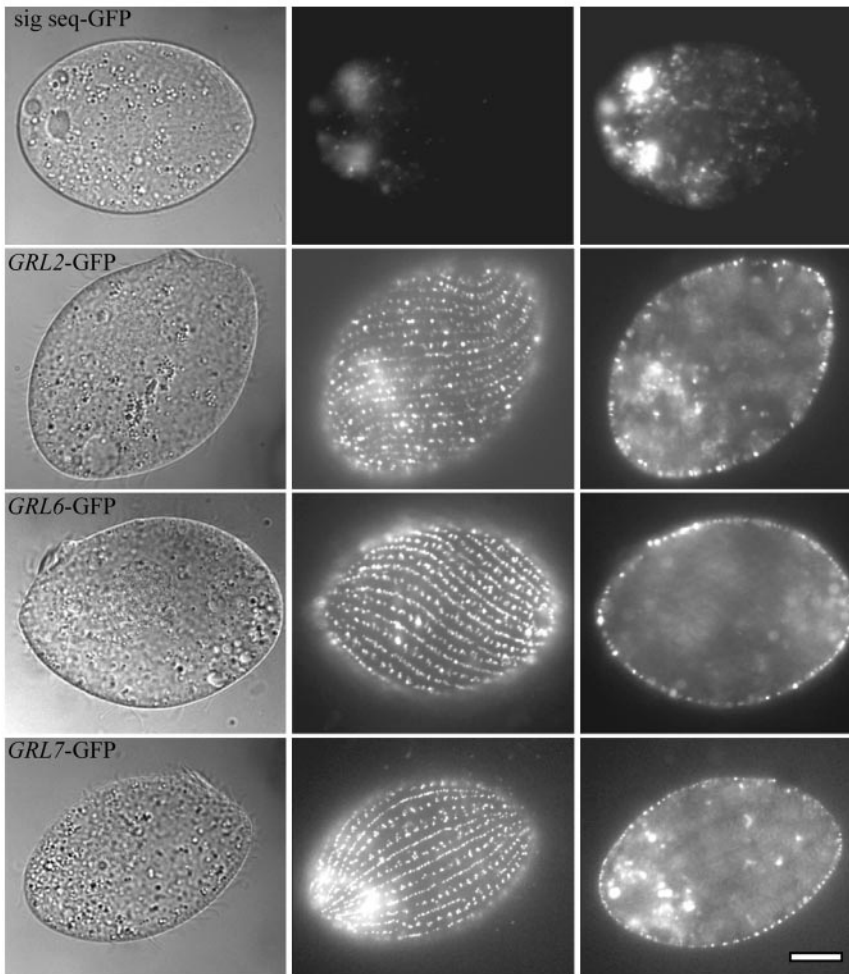


Figure 9. Localization of Grl2p and Grl6p to dense core granules by GFP chimeras. *GRL2* and *GRL6* were fused to GFP and expressed in growing cells. Shown for comparison are fusions of GFP with signal sequence alone (sig seq) or with a known granule content protein (*GRL7*). Bar, 10 μm .

these proteins accumulate in docked granules. Nonetheless, neither *GRL2* nor *6* is essential for DCG assembly and exocytic capsule formation, as shown via gene disruption (Figure 10). Both ΔGRL2 and ΔGRL6 cells were indistinguishable from wild type in Alcian Blue-stimulated capsule formation, which is a qualitative measure of exocytosis (Figure 11A). Exocytosis seemed to be as efficient as wild type, because ΔGRL2 and ΔGRL6 cells underwent complete degranulation after exposure to Alcian Blue as judged by immunofluorescence (our unpublished data). Consistent with this, electron microscopy (EM) analysis of fixed thin sections revealed docked DCGs with crystalline cores (Figure 11B). Based on these observations, we tentatively concluded that neither Grl2p nor Grl6p plays an important role in granulogenesis.

We were therefore surprised to observe that ΔGRL6 cells showed a large quantitative deficiency in exocytosis. When *Tetrahymena* are treated with the local anesthetic dibucaine, granule contents are released via exocytosis but do not form a capsule, as they do in the presence of Alcian Blue. Instead, the expanded granule lattices dissociate from the cells and form a sedimentable flocculent whose volume is many times greater than that of the cells themselves (Satir, 1977). Cell lines disrupted in *GRL1*, 3, 4, 7, or 8, or bearing a *GRL5* antisense insert, do not produce any visible flocculent when stimulated, because the granule cores in such cells do not expand upon exocytosis (Chilcoat *et al.*, 1996; our unpublished data). When ΔGRL6 cells were stimulated with dibucaine, the volume of the flocculent was reduced 40–70%

relative to wild type ($n = 10$) (our unpublished data). This smaller volume could result from the release of a smaller number of DCGs, or from DCGs containing cores that undergo more limited expansion than those in wild type. The latter was ruled out by measuring the protein content of the flocculent: ΔGRL6 cells not only released a smaller volume of flocculent than wild type, but it contained a correspondingly smaller amount of protein ($n = 2$) (our unpublished data). In fact, visualization of four independent ΔGRL6 lines by immunofluorescence of fixed cells demonstrated that they contain significantly fewer docked DCGs than in wild-type cells or other ΔGRL lines (Figure 12A).

The DCGs also seemed wider, when viewed en face, than those in wild type. To be certain that this was not a fixation artifact, we transformed wild-type, ΔGRL1 , ΔGRL2 , and ΔGRL6 cells with *Igr1p-GFP*, a fluorescent marker for DCGs (Haddad *et al.*, 2002). Analysis of docked DCGs in living cells confirmed that the ΔGRL6 DCGs are both shorter and wider than those in wild type, although clearly different from the spherical DCGs in ΔGRL1 (Figure 12B). ΔGRL2 DCGs were not distinguishable from wild type.

The difference in DCG accumulation also was supported by immunodetection of granule contents in whole cell lysates, because the amounts of several Grl proteins, in their processed forms, seemed reduced in ΔGRL6 cells relative to wild type or ΔGRL2 (Figure 12C). Unexpectedly, the ΔGRL6 cells also showed increased accumulation of the corresponding Grl proproteins. As discussed above, this could reflect

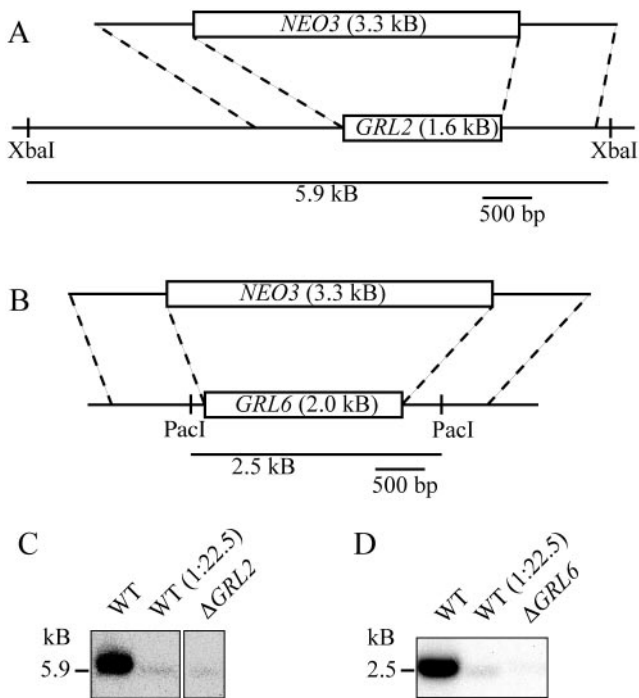


Figure 10. Disruption of *GRL2* and *GRL6* through homologous recombination. (A) *GRL2* genomic locus, showing the replacement by the MTT-NEO cassette of the entire *GRL2* ORF. (B) Southern blot of a *GRL2* knockout line, with a probe generated from the *GRL2* cDNA. The remaining material at the size of the wild-type locus is transcriptionally silent micronuclear DNA. (C) *GRL6* locus, showing the replacement by the MTT-NEO cassette of the entire *GRL6* ORF. (D) Southern blot of a *GRL6* knockout line, with a probe generated from the *GRL6* cDNA; the remaining signal is from detection of micronuclear DNA. We used Southern blotting, with a probe generated from the NEO marker, to confirm that Δ *GRL6* cells contained NEO at a single locus (our unpublished data).

either a transport or an assembly defect. Immunolocalization of Gr13p in these cells, using mAb 5E9, demonstrated that all detectable protein was present in the docked secretory granules, suggesting the latter (our unpublished data). It is important to note that these Western blots cannot be used to judge the relative levels of pro- and processed versions of each species, because some antibodies seem to be far more reactive on Western blots against the proprotein forms (Bowman and Turkewitz, unpublished). These results indicate that Gr13p plays an important role in DCG biogenesis. Given the fact that its absence alters core dimensions without eliminating lattice formation, and results in decreased

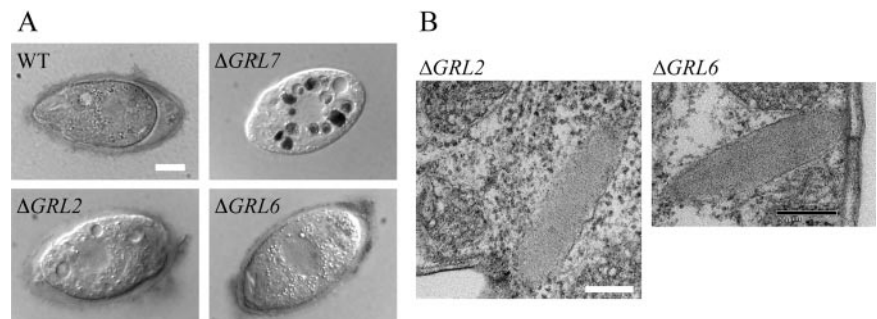
granule accumulation, we conclude that this role is different from that of the six major Gr1 proteins. Table 2 summarizes the phenotypes associated with the set of *GRL* disruptions.

Epistasis Analysis of *GRL6* Function

The reduction in granule accumulation in Δ *GRL6* cells could reflect a decreased rate of synthesis, if this relatively low abundance core protein normally acts as a master regulator. Alternatively, Δ *GRL6* granules could be synthesized at the same rate as wild type, but lost at an accelerated pace. Because we saw no indications of cytoplasmic granule degradation in light or electron micrographs of Δ *GRL6* cells, we hypothesized that such accelerated loss could occur by an increase in nonstimulated exocytosis. To explore this idea, we disrupted *GRL6* in a mutant cell line, MN173, in which granule transport to the plasma membrane is impaired (Figure 13A) (Melia *et al.*, 1998). As a result, MN173 cells accumulate secretory granules in the cytoplasm, rather than docking them at the plasma membrane. If *GRL6* is required for granule synthesis per se, MN173 Δ *GRL6* double mutants would be expected to accumulate fewer granules than MN173 itself. However, if Δ *GRL6* granules are lost from cells by premature exocytosis, this defect might be suppressed in the MN173 background, because such exocytosis requires that the granules first be docked at the plasma membrane.

Neither microscopy nor dibucaine-stimulated protein release could be readily used to assess granule abundance in the MN173 background, because granules are not docked at the cell surface. Instead, we used flow cytometry of fixed permeabilized cells that were immunostained with antibodies against either of two granule contents proteins, Gr1p and Gr13p. Using this approach, we first confirmed that Δ *GRL6* cells contain fewer granules than wild type (Figure 13B). Similar results were obtained using either antibody, and with cells from either stationary or starved cultures. For the double mutant analysis, we selected two lines derived from a single transformation in which we introduced a NEO-disrupted copy of *GRL6*. Drug-resistant clones derived from this transformation are expected to contain a variable number of the wild-type versus disrupted allele, during the several week interval during which the latter is driven to fixation (Turkewitz *et al.*, 2002). Southern analysis of these two lines shows that, in clone 7, the wild-type allele is still present at wild-type levels, whereas complete replacement by the null allele has occurred in clone 10 (Figure 13A). We measured granule content in these two clones. In striking contrast to the results of *GRL6* disruption in a wild-type background, the Δ *GRL6* MN173 cells (clone 10) showed no decrease in the accumulation of Gr13p, relative to clone 7 (Figure 13B). Interestingly, on average, MN173 cells lacking *GRL6* accumulated a somewhat higher level of both granule markers than MN173 cells with wild-type levels of *GRL6*

Figure 11. Phenotypic analysis of *GRL2* and *GRL6* knockout lines. (A) Encapsulation assay. Δ *GRL2* and Δ *GRL6* cells were starved and treated with the dye Alcian Blue to induce capsule formation. Shown for comparison are wild-type and Δ *GRL7* cells treated in the same manner. The dark circles in the Δ *GRL7* cell are food vacuoles filled with ingested dye. Bar, 10 μ m. (B) Electron micrographs of individual granules from Δ *GRL2* and Δ *GRL6* cells, showing that the contents are ordered. Bars, 0.2 μ m.



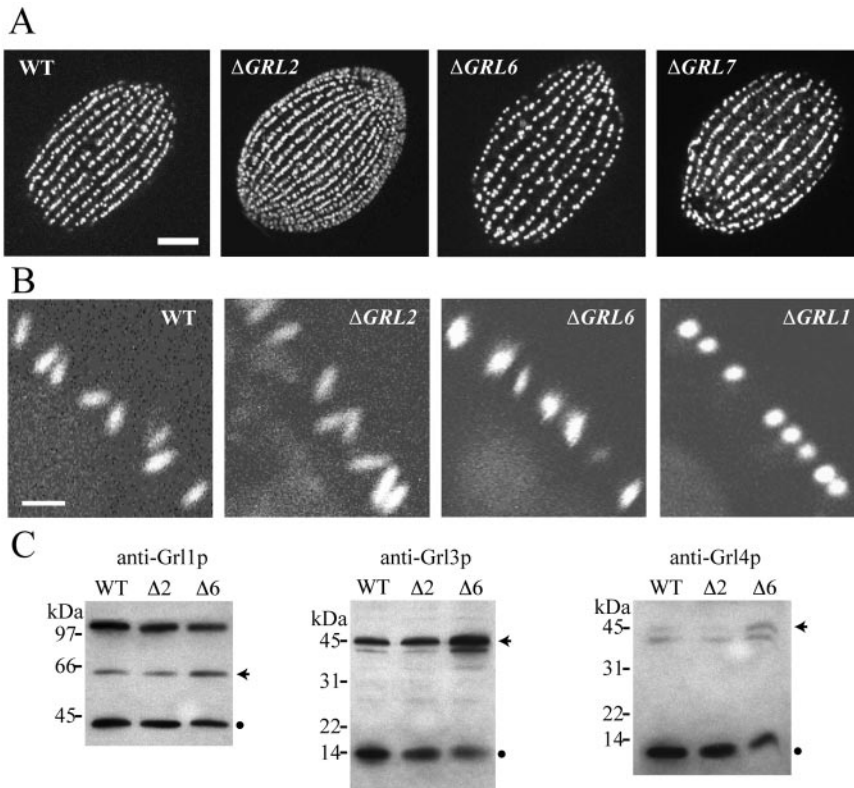


Figure 12. Granule synthesis defects in $\Delta GRL6$ cells. (A) Granules in stationary phase cells were visualized using indirect immunofluorescence and mAb 4D11. Wild-type, $\Delta GRL2$ and $\Delta GRL7$ cells all show a dense pattern of docked DCGs. The DCGs in $\Delta GRL6$ are comparatively sparse. Bar, 10 μm . (B) Images of live cells expressing Igr1p-GFP. Each image contains a cross-sectional view, showing the profiles of docked granules at the plasma membrane. The left side of the membrane faces the cytoplasm. Bar, 2 μm . (C) Immunodetection of Grl proteins (precursors and products) on Western blots of whole cell lysates. The bands corresponding to the precursor (arrow) and product (circle) of each Grl protein are indicated. $\Delta GRL6$ cells accumulate a higher level of each precursor, and a lower level of each product, relative to wild type. It is important to note that these blots cannot be used to compare the relative levels of pro- and processed versions of each species, because some antibodies seem to be far more reactive on Western blots against the proprotein forms (Bowman and Turkewitz, unpublished).

(Figure 13C). Immunofluorescence visualization of Grl3p in these cells showed the expected pattern of cytoplasmic granules, and identical flow cytometric results were obtained using either mAb 4D11 or 5E9, which recognize two different, unrelated granule markers (our unpublished data). These results do not support the idea that *GRL6* is required for efficient granule synthesis, because MN173 $\Delta GRL6$ cells show no deficiency in granule accumulation. Instead, they suggest that absence of Grl6p in an otherwise wild-type cell causes accelerated granule loss. This loss is likely to be via a process requiring transport to the plasma membrane, because the reduction in granule accumulation is suppressed in the MN173 background.

DISCUSSION

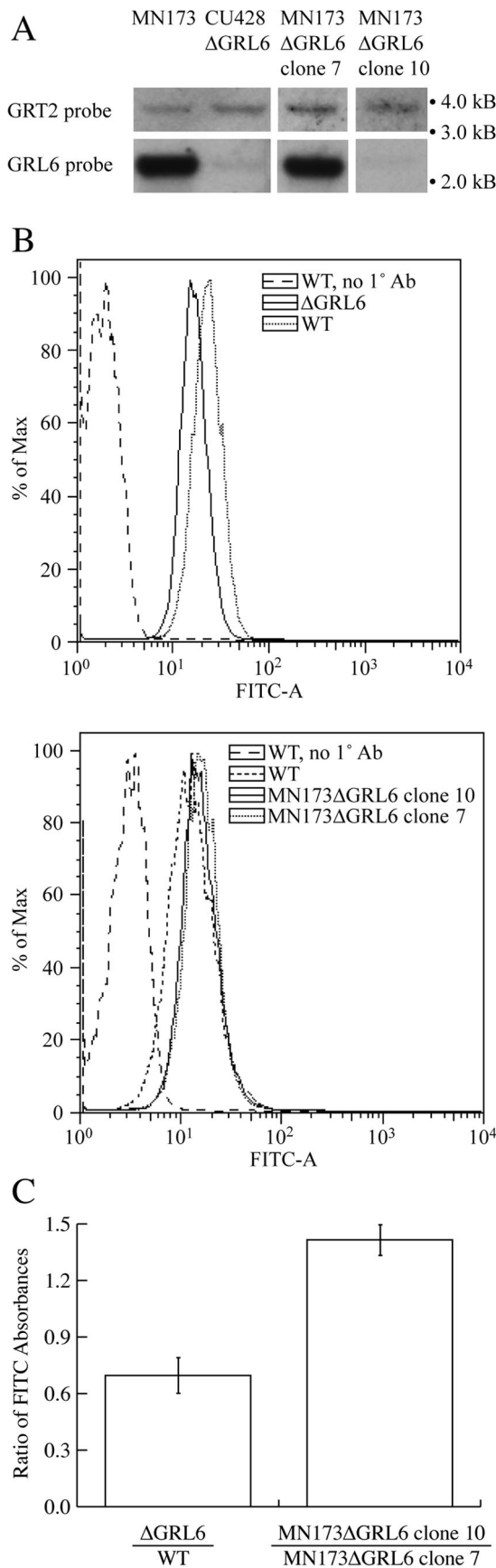
Ciliate DCG formation is driven by protein self-assembly into ordered multisubunit structures (Adoutte *et al.*, 1984). Our results indicate that *GRL1*, 3, 4, 5, 7, and 8 are essential for such assembly in *T. thermophila*. Because *Tetrahymena* granules clearly contain other proteins, their absence from the antisense screen output suggests they do not play essen-

tial nonredundant roles in core formation. At the same time, the results indicate limitations to this approach. An unbiased genetic screen would have been expected to yield mutations affecting multiple steps upstream of granule content release (Orias *et al.*, 1983; Melia *et al.*, 1998). The fact that only granule assembly mutants were recovered, linked to *GRL* deficiencies, reflects a bias for highly expressed genes, due to the fact that antisense libraries were constructed from pooled mRNAs. Thus, a conservative conclusion is that no other nonessential genes, expressed at levels comparable with the six *GRLs*, are essential for granulogenesis.

Our results reinforce reports that antisense sequences overlapping the 5' UTR are most effective, because all inserts we obtained met this criterion (Sweeney *et al.*, 1996; Jacobs *et al.*, 2004). The results also suggest useful modifications. First, library normalization could reduce representational biases due to transcript abundance. Second, modifying the transformation protocol to limit the uptake of antisense rDNAs could enhance this approach, because most transformants maintained multiple vectors. We focused on cells from which we recovered single antisense rDNAs. Our results hinted that many of these may have harbored additional

Table 2. Summary of *GRL* mutants

Gene mutation	Granule morphology	Granule no.	Rapid release of granule contents
None (wild type)	Elongated, crystalline core	Wild type	Yes
$\Delta GRL1$, 3, 4, 7, or 8 (macronuclear)	Spherical, amorphous core	~Wild type	No
$\Delta GRL2$ (macronuclear)	Elongated, crystalline core	~Wild type	Yes
$\Delta GRL6$ (macronuclear)	Shorter, wider than WT, crystalline core	Reduced	Yes
<i>GRL5</i> antisense	Spherical, amorphous core	~Wild type	No



inserts, however, because many of the recovered inserts did not regenerate exocytosis phenotypes. Because antisense ribosomes can suppress translation, even when present as a minority, we hypothesize that unrecovered inserts accounted for the exocytosis defects in such transformants. The simplest hypothesis is that these also corresponded to *GRL* genes.

In $\Delta GRL1$ or $\Delta GRL8$ cells, DCGs are spherical rather than elongated (Chilcoat *et al.*, 1996; Chilcoat *et al.*, 2001). The same was found here following disruption of *GRL3*, 4, or 7. These results suggest that each of the *Grl* proteins is distributed throughout a relatively uniform lattice. The possibility that six *Grl* proteins coassemble to form a repeating lattice subunit is consistent with the comparable abundance of five of the *GRL* products (Verbsky and Turkewitz, 1998). We infer that the sixth, *Grl8p*, is also abundant, because the gene is well represented in EST libraries.

Assembly of the DCG lattice begins early in the secretory pathway, because pro $Grl1p$ fails to exit the ER in a $\Delta GRL4$ strain, but not $\Delta GRL3$ or 8. This may serve as a mechanism to enhance the efficiency of lattice formation, by imposing a compartmentally controlled order of assembly, and may establish the stoichiometry of *Grl1p* and *Grl4p* products. This system is highly stringent, so that the accumulation of processed *Grl1p* is independent of the amount of pro $Grl1p$ available. The disruption of *GRL3* or *GRL8* partially inhibited pro $Grl1p$ processing. If we assume that all pro $Grl1p$ that exits the ER undergoes subsequent processing, this inhibition could reflect partial retention of pro $Grl1p$ in the ER. This would suggest that other pro Grl proteins contribute to transport of pro $Grl1p$, without being absolutely required. However, inhibition also can be explained if processing depends upon subsequent steps that are blocked in the mutants.

An attractive model of lattice assembly posits that soluble *Grl* (or *tmp*) precursors are delivered to immature granules, where processing generates assembly-competent products (Adoutte *et al.*, 1984; Vayssie *et al.*, 2001). However, in $\Delta GRL3$ and $\Delta GRL8$ cells, *Grl1p*-GFP seems overwhelmingly to accumulate in granules, and yet Western blots indicate significant accumulation of pro $Grl1p$. Second, pro $Grl1p$ evidently does not require processing to crystallize, because it does so in the ER when overexpressed. This recalls reports in

Figure 13. Epistasis analysis of *GRL6* function. (A) Southern blotting of whole cell DNA from wild type, $\Delta GRL6$ in the CU428 (WT) background (same strain as in Figure 10), and two clones of MN173 $\Delta GRL6$, using probes against *GRT2* (loading control) and *GRL6*. Clone 7 has maintained *GRL6* at wild-type levels, whereas clone 10 is equivalent to the established $\Delta GRL6$ strain. The remaining signal is due to the micronuclear *GRL6* copies, which are not expressed. (B) Flow cytometry of wild-type and $\Delta GRL6$ cells to quantify *Grl3p*, a granule marker. Shown are two trials. In the first, wild-type (WT) cells are compared with $\Delta GRL6$ cells, and the latter show a leftward shift representing a decrease in mean fluorescence per cell. In the second, wild-type cells are compared with MN173 clone 7 (wild-type level of *GRL6*) and clone 10 ($\Delta GRL6$). Mean fluorescence in the two clones is similar. In both panels, the left-most curve represents cells with no 1° antibody. Identical results were obtained using mAb 4D11, which recognizes granule marker *Grt2p*. (C) Effect of *GRL6* disruption on granule content. Shown is the ratio (mean, with SD) of FITC fluorescence in cells without *GRL6* versus with *GRL6*. Mean FITC fluorescence was measured by flow cytometry, as in B, in cells labeled with mAbs 4D11 or 5E9. On the left, the ratio of fluorescence in $\Delta GRL6$ cells versus wild type ($n = 7$). Disrupting *GRL6* results in a decrease in mean fluorescence. On the right, the ratio of fluorescence in MN173 $\Delta GRL6$ versus MN173 (clone 10 vs. clone 7) ($n = 5$). In the MN173 background, disruption of *GRL6* results in an increase in mean fluorescence.

which mammalian DCG proteins assembled in the ER or Golgi under stress conditions, reflecting the tendency of these proteins to crystallize (Tooze *et al.*, 1989). Although proGrl1p crystallization in the ER may not be physiological, assembly of proproteins is also suggested by images of immature granule-like vesicles in two mutants, UC620 and 623. These show very limited processing of proGrl proteins, but the cores nonetheless show regions organized as lattices (Bowman *et al.*, 2005). These results may be reconciled if processing, rather than acting before assembly, instead acts selectively upon proproteins that have recently assembled, thereby rendering the process irreversible. This model could account for the partial inhibition of proGrl1p processing in all ΔGRL strains, because the absence of any Grl protein would preclude formation of a subset of lattice contacts.

Although six *GRL* genes encode the basic lattice architecture, four additional related genes exist in the genome. Two (*GRL9* and *10*) are closely related to *GRL5*. Neither seems to be transcribed at a high level based on their absence from the EST database. Interestingly, analysis of amino acid substitution rates indicated that *GRL10* is evolving under elevated rates of amino acid substitution, strongly implicating the role of natural selection in its evolution. The significant deviation from $\omega = 1$ for *GRL10* provides strong evidence of nonneutral evolution (either purifying selection or directional selection), suggesting both that the gene is transcribed and that it confers a phenotype. In contrast, the substitution rates of *GRL5* and *GRL9* cannot be distinguished from the neutral evolution rate. For those genes, the observation of ω near 1 indicates only that *on average* the sequences in question cannot be distinguished from the neutral rate. This is compatible with either all codons evolving at a rate such that ω is near 1, or a subset of codons evolving under constraint with others evolving under natural selection and/or neutrality such that the average ω is near 1.

GRL2 and *6* were analyzed by several criteria. The GFP-tagged proteins were targeted to DCGs, but the endogenous genes are transcribed at <5% the level of the major *GRLs*. Consistent with this, gene disruption revealed that neither is required to form exocytosis-competent DCGs. Nonetheless, disruption of *GRL6* had a remarkable effect on the size of the exocytic response, reducing the amount of material released, as well as changing granule morphology. The former seems primarily due to a reduction in DCG number. For some mammalian cells, specific cargo proteins, namely, members of the chromogranin family, may play important roles in determining granule number (Kim *et al.*, 2001). The mechanisms are unknown, but chromogranins are major structural components of dense cores (Chanat *et al.*, 1991). The $\Delta GRL6$ phenotype is consistent with this idea, but with the important difference that Grl6p is apparently present at relatively low levels. This estimate of protein scarcity is inferred from transcript abundance, and is consistent with the fact that no *GRL6* products have been detected as major granule components. Several different phenomena might contribute to DCG reduction in $\Delta GRL6$ cells. Grl6p could be a master regulator of *GRL* gene expression, or might be required for correct targeting of the major core proteins. A third possibility is that $\Delta GRL6$ DCGs are synthesized at wild-type levels but are unstable. An elevated level of DCG loss, due to a high level of unstimulated exocytosis, would result in low steady-state accumulation. Consistent with the last model, and inconsistent with the first two, we found that the decrease in granule accumulation in $\Delta GRL6$ cells was suppressed in the background of a second mutation that inhibits efficient transport of granules to the plasma membrane. We propose that unstimulated exocytosis of $\Delta GRL6$ granules

reflects a change, relative to wild-type, in the distribution of proteins in the secretory granule membrane. Grl6p may be distributed at the periphery of the wild-type granule lattice, in a position where its absence might affect, directly or indirectly, the recruitment or retention of transmembrane proteins. A change in membrane protein composition also may account for the superaccumulation of granules in MN173 $\Delta GRL6$ cells, but the extent and mechanism of granule turnover in MN173 cells are as yet unknown. The limited data on membrane proteins of dense core granules suggest that interactions with luminal proteins may provide one important mechanism for sorting, but the specificity of those interactions is unclear (Wasmeier *et al.*, 2002). Our *in vivo* data on defects in ΔGRL granules may suggest that, within this protein family, a subset of members may be adapted less for structural roles within the core lattice than for interactions with nonlattice proteins and may provide an interesting new perspective on secretory granule formation.

ACKNOWLEDGMENTS

We thank members of this laboratory, including N. D. Chilcoat and J. Verbsky for contributions to analysis of ΔGRL strains; A. Sitikov for construction of antisense libraries; and N. Elde, N. Bradshaw, and M. Nasone for discussion and support. James Marvin and Ryan Duggan (Cancer Research Center Flow Cytometry Facility, University of Chicago) provided invaluable technical support and advice. J.J.E. acknowledges helpful discussion with Ying Chen and Kevin Thornton. Lawrence Klobutcher (University of Connecticut, Storrs, CT) shared valuable ideas on antisense library construction. The NEO3 construct and the *MTT1* promoter construct were generously provided by M. Gorovsky (University of Rochester, Rochester, NY), and the 4D11 and 5E9 hybridomas were a gift of Marlo Nelson and Joseph Frankel (University of Iowa). We thank Yimei Chen and The University of Chicago EM facility, and the Cancer Research Center, for electron microscopy. A.T.C. and G.R.B. were supported, respectively, by Training Grants GM-07281 and GM-07183. J.J.E. was supported by a National Science Foundation Graduate research fellowship. This work was supported by National Institutes of Health Grants GM-50946 and GM-59268 (to A.P.T.).

REFERENCES

- Adoutte, A., Garreau de Loubresse, N., and Beisson, J. (1984). Proteolytic cleavage and maturation of the crystalline secretion products of *Paramecium*. *J. Mol. Biol.* *180*, 1065–1081.
- Andres, D. A., Rhodes, J. D., Meisel, R. L., and Dixon, J. E. (1991). Characterization of the carboxyl-terminal sequences responsible for protein retention in the endoplasmic reticulum. *J. Biol. Chem.* *266*, 14277–14282.
- Arvan, P., and Castle, D. (1998). Sorting and storage during secretory granule biogenesis: looking backward and looking forward. *Biochem. J.* *332*, 593–610.
- Arvan, P., and Castle, J. D. (1992). Protein sorting and secretion granule formation in regulated secretory cells. *Trends Cell. Biol.* *2*, 327–331.
- Arvan, P., Zhang, B. Y., Feng, L., Liu, M., and Kuliawat, R. (2002). Luminal protein multimerization in the distal secretory pathway/secretory granules. *Curr. Opin. Cell Biol.* *14*, 448–453.
- Bowman, G. R., Elde, N. C., Morgan, G., Winey, M., and Turkewitz, A. P. (2005). Core formation and the acquisition of fusion competence are linked during secretory granule maturation in *Tetrahymena*. *Traffic* *6*, 303–323.
- Bowman, G. R., and Turkewitz, A. P. (2001). Analysis of a mutant exhibiting conditional sorting to dense core secretory granules in *Tetrahymena thermophila*. *Genetics* *159*, 1605–1616.
- Bradshaw, N. R., Chilcoat, N. D., Verbsky, J. W., and Turkewitz, A. P. (2003). Proprotein processing within secretory dense core granules of *Tetrahymena thermophila*. *J. Biol. Chem.* *278*, 4087–4095.
- Chanat, E., and Huttner, W. B. (1991). Milieu-induced, selective aggregation of regulated secretory proteins in the trans-Golgi network. *J. Cell Biol.* *115*, 1505–1519.
- Chanat, E., Martin, P., and Ollivier-Bousquet, M. (1999). Alpha(S1)-casein is required for the efficient transport of β - and κ -casein from the endoplasmic reticulum to the Golgi apparatus of mammary epithelial cells. *J. Cell Sci.* *112*, 3399–3412.

- Chanat, E., Pimplikar, S. W., Stinchcombe, J. C., and Huttner, W. B. (1991). What the granins tell us about the formation of secretory granules in neuroendocrine cells. *Cell Biophys.* *19*, 85–91.
- Chilcoat, N. D., Elde, N. C., and Turkewitz, A. P. (2001). An antisense approach to phenotype-based gene cloning in *Tetrahymena*. *Proc. Natl. Acad. Sci. USA* *98*, 8709–8713.
- Chilcoat, N. D., Melia, S. M., Haddad, A., and Turkewitz, A. P. (1996). Granule lattice protein 1 (Gr1p), an acidic, calcium-binding protein in *Tetrahymena thermophila* dense-core secretory granules, influences granule size, shape, content organization, and release but not protein sorting or condensation. *J. Cell Biol.* *135*, 1775–1787.
- Dhanvantari, S., and Loh, Y. P. (2000). Lipid raft association of carboxypeptidase E is necessary for its function as a regulated secretory pathway sorting receptor. *J. Biol. Chem.* *275*, 29887–29893.
- Farrell, R.E.J. (1993). *RNA Methodologies: A Laboratory Guide for the Isolation and Characterization*, New York: Academic Press.
- Frankel, J. (2000). Cell biology of *Tetrahymena thermophila*. *Methods Cell Biol.* *62*, 27–125.
- Gaertig, J., and Gorovsky, M. A. (1995). DNA mediated transformation in *Tetrahymena*. In: *Cilia and Eukaryotic Flagella*, vol. 47, ed. W. Dentler, New York: Academic, 559–569.
- Gaertig, J., Gu, L., Hai, B., and Gorovsky, M. A. (1994). High frequency vector-mediated transformation and gene replacement in *Tetrahymena*. *Nucleic Acids Res.* *22*, 5391–5398.
- Gautier, M.-C., Sperling, L., and Madeddu, L. (1996). Cloning and sequence analysis of genes coding for *Paramecium* secretory granule (trichocyst) proteins. *J. Biol. Chem.* *271*, 10247–10255.
- Haddad, A., Bowman, G. R., and Turkewitz, A. P. (2002). New class of cargo protein in *Tetrahymena thermophila* dense core secretory granules. *Eukaryot. Cell* *1*, 583–593.
- Hausmann, K. (1978). Extrusive organelles in protists. *Int. Rev. Cytol.* *52*, 197–276.
- Jacobs, M. E., Cortezzo, D. E., and Klobutcher, L. A. (2004). Assessing the effectiveness of coding and non-coding regions in antisense ribosome inhibition of gene expression in *Tetrahymena*. *J. Eukaryot. Microbiol.* *51*, 536–541.
- Kim, T., Tao-Cheng, J. H., Eiden, L. E., and Loh, Y. P. (2001). Chromogranin A, an “on/off” switch controlling dense-core secretory granule biogenesis. *Cell* *106*, 499–509.
- Madeddu, L., Gautier, M.-C., Vayssié, L., Houari, A., and Sperling, L. (1995). A large multigenic family codes for the polypeptides of the crystalline trichocyst matrix in *Paramecium*. *Mol. Biol. Cell* *6*, 649–659.
- Melia, S. M., Cole, E. S., and Turkewitz, A. P. (1998). Mutational analysis of regulated exocytosis in *Tetrahymena*. *J. Cell Sci.* *111*, 131–140.
- Orias, E., Flacks, M., and Satir, B. H. (1983). Isolation and ultrastructural characterization of secretory mutants of *Tetrahymena thermophila*. *J. Cell Sci.* *64*, 49–67.
- Rosati, G., and Modeo, L. (2003). Extrusomes in ciliates: diversification, distribution, and phylogenetic implications. *J. Eukaryot. Microbiol.* *50*, 383–402.
- Satir, B. (1977). Dibucaine-induced synchronous mucocyst secretion in *Tetrahymena*. *Cell Biol. Int. Rep.* *1*, 69–73.
- Shang, Y., Song, X., Bowen, J., Corstanje, R., Gao, Y., Gaertig, J., and Gorovsky, M. A. (2002). A robust inducible-repressible promoter greatly facilitates gene knockouts, conditional expression, and overexpression of homologous and heterologous genes in *Tetrahymena thermophila*. *Proc. Natl. Acad. Sci. USA* *99*, 3734–3739.
- Sweeney, R., Fan, Q., and Yao, M.-C. (1996). Antisense ribosomes: rRNA as a vehicle for antisense RNAs. *Proc. Natl. Acad. Sci. USA* *93*, 8518–8523.
- Tooze, J., Kern, H. F., Fuller, S. D., and Howell, K. E. (1989). Condensation-sorting events in the rough endoplasmic reticulum of exocrine pancreatic cells. *J. Cell Biol.* *109*, 35–50.
- Tooze, S. A., Martens, G. J., and Huttner, W. B. (2001). Secretory granule biogenesis: rafting to the SNARE. *Trends Cell Biol.* *11*, 116–122.
- Turkewitz, A. P. (2004). Out with a bang! *Tetrahymena* as a model system to study secretory granule biogenesis. *Traffic* *5*, 63–68.
- Turkewitz, A. P., Chilcoat, N. D., Haddad, A., and Verbsky, J. W. (2000). Regulated protein secretion in *Tetrahymena thermophila*. *Methods Cell Biol.* *62*, 347–362.
- Turkewitz, A. P., and Kelly, R. B. (1992). Immunocytochemical analysis of secretion mutants of *Tetrahymena* using a mucocyst-specific mAb. *Dev. Genet.* *13*, 151–159.
- Turkewitz, A. P., Madeddu, L., and Kelly, R. B. (1991). Maturation of dense core granules in wild type and mutant *Tetrahymena thermophila*. *EMBO J.* *10*, 1979–1987.
- Turkewitz, A. P., Orias, E., and Kapler, G. (2002). Functional genomics: the coming of age for *Tetrahymena thermophila*. *Trends Genet.* *18*, 35–40.
- Vayssie, L., Garreau De Loubresse, N., and Sperling, L. (2001). Growth and form of secretory granules involves stepwise assembly but not differential sorting of a family of secretory proteins in *Paramecium*. *J. Cell Sci.* *114*, 875–886.
- Vayssie, L., Skouri, F., Sperling, L., and Cohen, J. (2000). Molecular genetics of regulated secretion in *Paramecium*. *Biochimie* *82*, 269–288.
- Verbsky, J. W., and Turkewitz, A. P. (1998). Proteolytic processing and Ca²⁺-binding activity of dense-core vesicle polypeptides in *Tetrahymena*. *Mol. Biol. Cell* *9*, 497–511.
- Wasmeier, C., Bright, N. A., and Hutton, J. C. (2002). The luminal domain of the integral membrane protein phogrin mediates targeting to secretory granules. *Traffic* *3*, 654–665.
- Yang, Z. (1998). Likelihood ratio tests for detecting positive selection and application to primate lysozyme evolution. *Mol. Biol. Evol.* *15*, 568–573.